AGU100 ADVANCING EARTH AND SPACE SCIENCE

Geochemistry, Geophysics, Geosystems

TECHNICAL REPORTS: METHODS

10.1029/2017GC007412

Key Points:
- We present two xenotime primary reference materials (XN01 and XN02) for U-Pb LA-ICP-MS geochronology
- We provide Isotope Dilution-Thermal Ionization Mass Spectrometry (ID-TIMS) U-Pb isotope reference values for XN01 and XN02
- We present additional xenotime (XN03, XN04, and XN05) as ideal candidates for further U-Pb ID-TIMS geochronology

Supporting Information:
- Supporting information S1
- Table S1
- Table S2
- Table S3
- Table S4
- Table S5
- Table S6
- Table S7

Correspondence to:
G. O. Gonçalves,
goncalves.go@icloud.com

Citation:
Vasconcelos, A. D., Gonçalves, G. O., Lana, C., Buick, I. S., Kamo, S. L., Corfu, F., et al. (2018). Characterization of xenotime from Datas (Brazil) as a potential reference material for in situ U-Pb geochronology. *Geochemistry, Geophysics, Geosystems*, *19*, 2262–2282. https://doi.org/10.1029/2017GC007412

Received 16 JAN 2018
Accepted 1 JUN 2018
Accepted article online 26 JUN 2018
Published online 16 JUL 2018

Characterization of Xenotime From Datas (Brazil) as a Potential Reference Material for In Situ U-Pb Geochronology

A. D. Vasconcelos[1], G. O. Gonçalves[1], C. Lana[1], I. S. Buick[2], S. L. Kamo[3], F. Corfu[4], R. Scholz[1], A. Alkmim[1], G. Queiroga[1], and H. A. Nalini Jr.[1]

[1]Applied Isotope Research Group, Departamento de Geologia, Escola de Minas, Universidade Federal de Ouro Preto, Campus Universitário Morro do Cruzeiro, Ouro Preto, Brazil, [2]Department of Earth Sciences, Stellenbosch University, Matieland, South Africa, [3]Jack Satterly Geochronology Laboratory, Department of Earth Sciences, University of Toronto, Toronto, Ontario, Canada, [4]Department of Geosciences, University of Oslo, Oslo, Norway

Abstract This study investigates five megacrysts of xenotime (XN01, XN02, XN03, XN04, and XN05) as potential reference materials (RMs) for U-Pb geochronology. These crystals belong to a 300 g xenotime assortment, collected from alluvial deposits in SE Brazil. Electron microprobe and Laser Ablation-Inductively Coupled Plasma-Mass Spectrometry (LA-ICP-MS) analyses show that the selected crystals are internally homogeneous for most rare earth element, (REE, except some light REE) but are relatively heterogeneous for U and Th. The xenotime REE patterns are consistent with an origin from hydrothermal quartz veins in the Datas area that cut greenschist-facies metasediments and that locally contain other accessory phases such as rutile and monazite. High-precision U-Pb Isotope Dilution-Thermal Ionization Mass Spectrometry (ID-TIMS) analyses showed slight age heterogeneity for the XN01 crystal not observed in the XN02 sample. The two crystals have slightly different average $^{206}Pb/^{238}U$ ages of 513.4 ± 0.5 Ma (2 s) and 515.4 ± 0.2 Ma (2 s), respectively. In situ U-Pb isotope data acquired via LA-(Q,SF,MC)-ICP-MS are within the uncertainty of the ID-TIMS data, showing homogeneity at the 1% precision of the laser ablation (and probably ion microprobe) technique. U-Pb LA-(MC, SF)-ICP-MS analyses, using XN01 as a primary RM, reproduced the ages of other established RMs within less than 1% deviation. Other Datas crystals (XN03-05) also display a reproducibility in Pb/U dates better than 1% on LA-ICP-MS, making them good candidates for further testing by ID-TIMS.

1. Introduction

Given their commonly high U and Th, low common Pb contents, and low Pb-diffusivities, minerals such as zircon, monazite, and xenotime are valuable chronometers for dating a wide range of geological processes (e.g., diagenesis, magmatic crystallization, (poly) metamorphism, and/or hydrothermal mineralization), as well as for characterizing the provenance of sedimentary materials. Xenotime ([Y, heavy rare earth element, HREE]PO_4) is the least common of these accessory minerals, but it occurs in several geological environments, including as a detrital heavy mineral (Emden et al., 1997), as diagenetic overgrowths on zircon in sedimentary rocks (Rasmussen, 2005; Rasmussen et al., 2004), as a metamorphic accessory phase in lower greenschist- to granulite-facies metapelitic rocks (Hetherington et al., 2008; Rasmussen et al., 2010, 2011), as magmatic crystals in peraluminous felsic igneous rocks (Förster, 1998) and, rarely, in carbonatites (Wall et al., 2008), and in hydrothermal veins or mineralization (Hazarika et al., 2017; Rasmussen et al., 2007). It is considered a robust mineral for U-Th-Pb geochronology because of its favorable U-Th-Pb composition, high U, and low common Pb contents (Rasmussen et al., 2010), as well as its low Pb diffusivity over geological timescales, at least for temperatures below 750 °C (Cherniak, 2006; Dahl, 1997).

As with other accessory phases (e.g., monazite, zircon, titanite, and allanite/rare earth element [REE]-epidote; Bea & Monteiro, 1999; Buick et al., 2006; Dalquist, 2001; Fisher et al., 2017; Gregory et al., 2009; Storkey et al., 2005), xenotime compositions and their derivatives, including chondrite-normalized REE patterns and Eu anomalies, can be used to link its growth to that of other datable accessory phases, or major silicate mineral assemblages of known petrogenetic significance and, potentially, to distinguish between hydrothermal, subsolidus, and suprasolidus origins (e.g., Aleinikoff et al., 2012, 2015). In metamorphic and/or felsic magmatic rocks, xenotime may buffer the Y and HREE content of coexisting minerals, thus forming a basis for geothermometry (e.g., xenotime-buffered Y-in-garnet thermometry: Pyle & Spear, 2000; monazite-xenotime Y- and HREE- solvus geothermometry: Andrehs & Heinrich, 1998; Heinrich et al., 1997; Viskupic & Hodges, 2001).

Xenotime U-Pb geochronology usually requires an instrumental approach that provides high spatial resolution (e.g., in situ dating) because of well-known textural complexities. For example, diagenetic xenotime overgrowths on zircon are commonly narrower than 20–40 μm (e.g., Rasmussen et al., 2007), while, in felsic magmatic rocks, xenotime may contain xenocrystic cores and magmatic overgrowths that are difficult to separate physically (Miller et al., 1992). Xenotime grains in metamorphic rocks may contain multiple domains of different ages and chemical composition (e.g., Aleinikoff et al., 2012; Rasmussen et al., 2011; Viskupic & Hodges, 2001) since it is susceptible to fluid-mediated dissolution-reprecipitation or dissolution-replacement reactions (Švecová et al., 2016). Thus, the majority of xenotime high spatial resolution dating has been undertaken by either secondary ionization mass spectrometry (SIMS, mostly through SHRIMP-II instruments; e.g., Rasmussen et al., 2007, 2001) or through EPMA chemical dating (e.g., Hetherington et al., 2008). The latter method cannot assess concordance in the U-Pb isotope system.

Perhaps one of the main problems in dating xenotime (or other minerals) via in situ methods is the availability of matrix-matched reference materials (RMs) for calibration and quality control. In situ U-Pb measurements rely on external calibrations, which are invariably done using the standard-bracketing method, and use one or more additional matrix-matched RMs for quality control purposes. Even though matrix corrections can be applied for elemental mismatch (e.g., Fletcher et al., 2004), it is preferable to avoid further *sources of uncertainty* when possible. With the ever-increasing number of Laser Ablation-Inductively Coupled Plasma-Mass Spectrometry (LA-ICP-MS) instruments, there is therefore a constant need to develop matrix-matched RMs for U-Pb geochronology and isotope geochemistry in general. Nonmatrix-matched dating of xenotime by LA-ICP-MS, using zircon as the primary calibrant, for example, has been shown to result in significant matrix effects and the calculation of incorrect ages (Liu et al., 2011). Moreover, the search for reliable RMs has escalated because of the popularity of LA-ICP-MS U-Pb geochronology, which consumes relatively large amounts of RMs compared to SIMS or EPMA.

There are currently only three internationally distributed RMs for xenotime U-Pb geochronology. These are the MG-1 and BS-1 xenotime crystals described by Fletcher et al. (2004), dated at 490 ± 0.3 and 508.9 ± 0.3 Ma, respectively, and the z6413 xenotime of Stern and Rayner (2003), dated at 993.8 ± 0.7 Ma. These materials are primarily used in SHRIMP laboratories and are generally not available in sufficient quantities to distribute to LA-ICP-MS groups. Moreover, the existing standards vary significantly in U and Th contents (Fletcher et al., 2004), and the extent to which the major element composition of xenotime RM may cause matrix effects for LA-ICP-MS U-Pb geochronology, as appears to be the case for SIMS-based studies (Fletcher et al., 2004, 2000), also needs to be addressed. Therefore, there is a clear demand to be met for the development of new xenotime RMs for U-Pb geochronology.

In this paper, we characterize xenotime crystals from Southern Espinhaço Range, SE Brazil, as a potential RM for U-Pb geochronology. The Southern Espinhaço Range is the fold and thrust belt of the Araçuaí Orogen (AO; Alkmim et al., 2006). It is marked by a wide range of mineral deposits (e.g., hyaline quartz, tourmaline, and gemstones) associated with extensive hydrothermal fluid flow at circa 495–515 Ma (Gonçalves et al., 2017). More recently Gonçalves et al. (2018) described homogeneous, circa 495 Ma hydrothermal monazite crystals from the Diamantina region that have been proposed to be suitable RM for U-Pb geochronology by LA-ICP-MS and/or SIMS techniques. The xenotime crystals studied herein are from the same area and likely formed in similar hydrothermal quartz vein deposits. They occur as centimeter-diameter, gem-quality megacrysts and are relatively easy to obtain in high enough quantities for distribution to LA-ICP-MS laboratories. However, individual megacrysts from these deposits have not previously been studied and require characterization for chemical homogeneity tests via in situ techniques to assess their suitability as U-Pb RMs, followed by high-precision TIMS U-Pb geochronology.

2. Sample Provenance

Samples for this study were donated by the Museu de Ciência e Tecnologia da Escola de Minas de Ouro Preto, Minas Gerais, Brazil. They comprise an approximately 300 g assortment of loose xenotime crystals that were collected from alluvial deposits (approximately at 18°25′10″S latitude and 43°38′35″W longitude), probably sourced from quartz veins, near the cities of Datas and Diamantina in the southern portion of the Espinhaço Range (Figure 1). Such hydrothermal quartz veins crosscut the collisional fabrics of Proterozoic

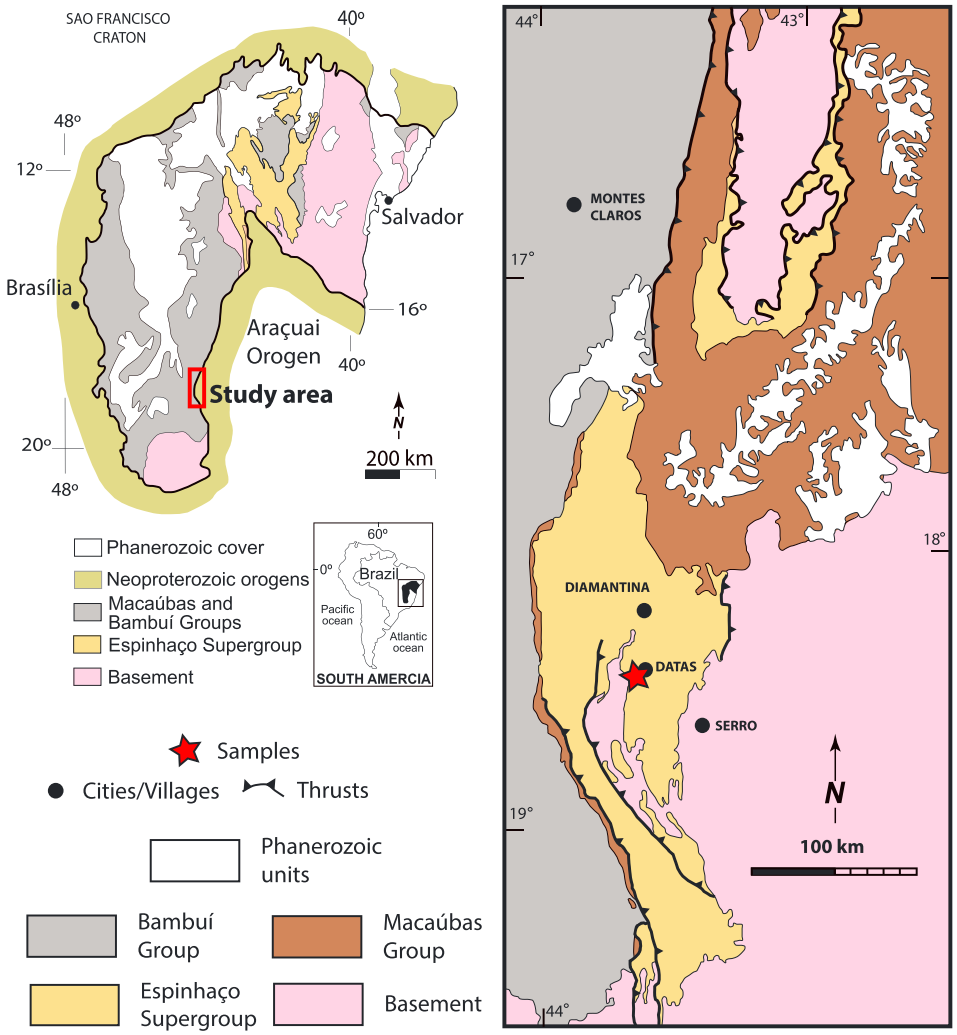

Figure 1. Geological map of the Southern Espinhaço Range in the eastern margin of the São Francisco Craton (top). The locality of the alluvial deposits with xenotime is represented by a red star (right). Modified from Alkmim and Martins-Neto (2012, and references therein).

Table 1
Summary of the Techniques Used in the Characterization of the Datas Xenotime Crystals

Summary of analyses							
Technique/ Facility	Chemical composition (LA-SF-ICP-MS)	Chemical composition (EPMA)	ID-TIMS U-Pb dating		LA-Q-ICP-MS U-Pb dating	LA-SF-ICP-MS U-Pb dating	LA-MC-ICP-MS U-Pb dating
	UFOP	UFOP	Toronto	Oslo	UFOP	UFOP	UFOP
XN01	10	22	3	2	15	25	16
XN02	10	33	3	2	15	18	21
XN03	10	18	—	—	13	31	60
XN04	10	11	—	—	9	26	6
XN05	10	16	—	—	13	25	8

Note. The values refer to the number of laser ablation spots or ID-TIMS aliquots analyzed. LA-ICP-MS = Laser Ablation-Inductively Coupled Plasma-Mass Spectrometry; Q = quadrupole; SF = sector field single collector; MC = multicollector; UFOP = Universidade Federal de Ouro Preto; EMPA = electron microprobe analyzer; ID-TIMS = Isotope Dilution-Thermal Ionization Mass Spectrometry.

Figure 2. (a) Datas xenotime crystals are brown in color and have subhedral shapes. (b) XN02 crystal fragments (like those selected for the epoxy mounts and Isotope Dilution-Thermal Ionization Mass Spectrometry analyses) showing a brown-honey color.

metasedimentary sequences of the Rio Paraúna (Paleoproterozoic) and Espinhaço (Mesoproterozoic to early Neoproterozoic; Chemale et al., 2012) Supergroups and carry accessory minerals such as rutile, anatase, brookite, xenotime-(Y), and rare monazite-(Ce). Regional studies, coupled with mineral geochemistry, have related these quartz veins to multiple episodes of devolatilization during folding and metamorphism at circa 500 Ma (Scholz et al., 2012).

3. Analytical Methods

Major and trace element compositions and U-Pb isotope analyses were obtained independently using a range of instruments at several institutions (Table 1). For this study, we have selected five well-shaped, euhedral to subhedral 1 to 2 cm long crystals (named XN01 to XN05). The crystals were then broken, and the selected transparent shards were mounted on double-sided tape, cast in 2.5 cm diameter epoxy resin mounts and then polished to obtain a flat surface suitable for different techniques. Two mounts were prepared, one with three to four random fragments from each crystal (hereafter referred as M1) and another one with the crystal XN03 (hereafter M2). Imaging and isotopic compositions were determined in both mounts, while chemical compositions were determined on mount M1. The high-precision U-Pb Isotope Dilution-Thermal Ionization Mass Spectrometry (ID-TIMS) data were obtained from two random fragments of the same crystals that were used to prepare mount M1. Backscattered electron (BSE) images were acquired using a JSM-6510 JEOL scanning electron microscope and chemical compositions were obtained by a JXA-8230 JEOL electron microprobe analyzer (EMPA) equipped with five wavelength-dispersive system spectrometers at the Universidade Federal de Ouro Preto (UFOP) in the Laboratório de Microanálises. Chemical compositions were also obtained using an Element II SF-ICP-MS, coupled with a G2-PhotonMachines excimer (193 nm) laser ablation system (e.g., Santos et al., 2017) at the Laboratório de Geoquímica (UFOP). U-Pb ages were obtained using quadrupole, sector field single collector, and multicollector ICP-MS instruments (LA-Q-ICP-MS, LA-SF-ICP-MS and LA-MC-ICP-MS) at UFOP (e.g., Gonçalves et al.,

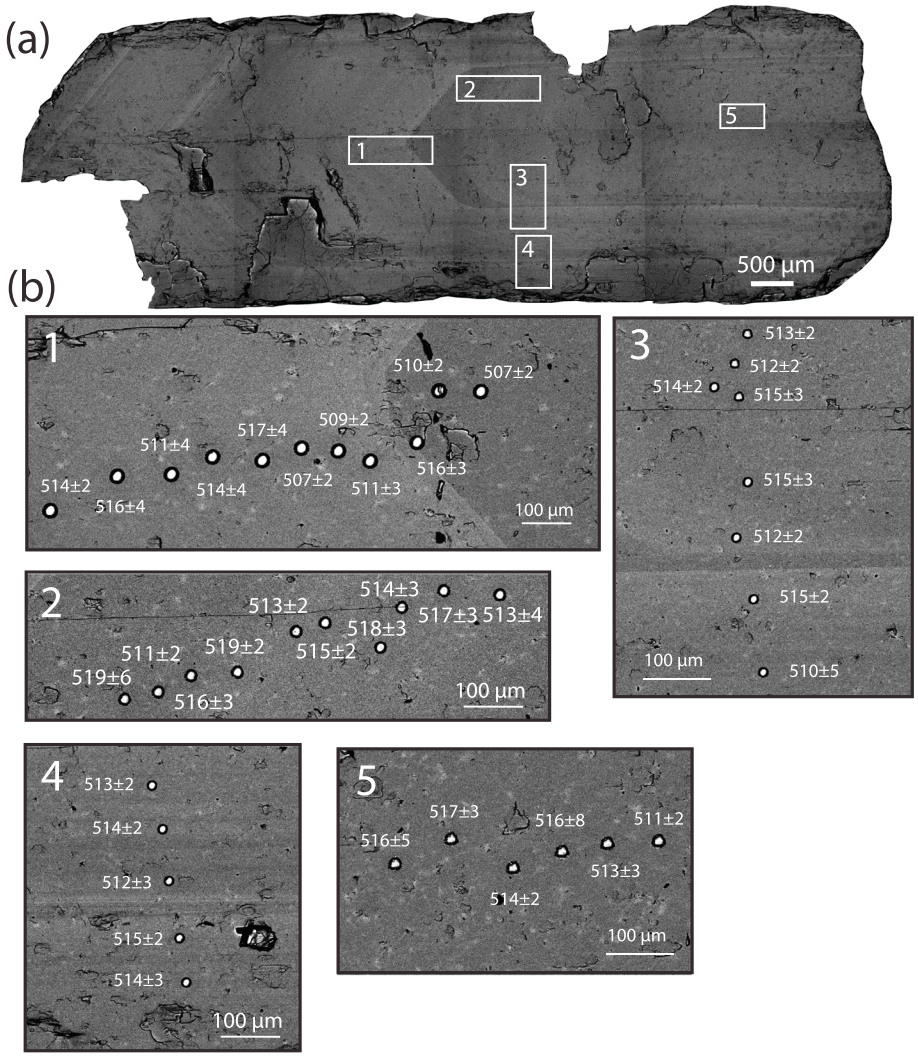

Figure 3. (a) BSE image of one of the Datas megacrysts (XN03) showing an oscillatory zoning and fractured domains. The white numbered squares represent Laser Ablation-multicollector-Inductively Coupled Plasma-Mass Spectrometry U-Pb laser ablation traverses (see section 4.2), shown in detail in the lower part of the figure (b). Each laser ablation spot is of 20 µm in diameter, while the apparent $^{206}Pb/^{238}U$ spot dates in Ma are given with 2-s uncertainties. BSE images of the other profiles are available in the supporting information. BSE = backscattered electron.

2018; Santos et al., 2017; Takenaka et al., 2015). The U-Pb measurements were undertaken in automated mode, with a spatial resolution of 20–30 µm. The $^{206}Pb/^{238}U$, $^{207}Pb/^{235}U$, and $^{207}Pb/^{206}Pb$ ratios were normalized against our primary RM MG-1 (Fletcher et al., 2004). The BS-1 xenotime (Fletcher et al., 2004) was used as secondary RM. The ID-TIMS U-Pb isotope ratios and ages were determined at the University of Toronto's Jack Satterly Geochronology Laboratory (JSGL, Canada) and the University of Oslo (Norway) using a VG354 and a MAT262 TIMS, respectively. A full description on the instrumentation and analytical conditions is given in the supporting information (Gerstenberger & Haase, 1997; Gerdes & Zeh, 2006, 2009; Gonçalves et al., 2016; Hiess et al., 2012; Ludwig, 2003; Stacey & Kramers, 1975; Van Achterbergh et al., 2001).

4. Results

4.1. Mineralogical and Chemical Characterization

The acquired batch of xenotime contains crystals that are variably euhedral to subhedral and range from a few millimeters to several centimeters in length. The five crystals selected for this study are brown, mostly

Table 2
Summary of the Electron Microprobe Results of the M1 Mount

Sample	XN01 (n = 22)	1 s	XN02 (n = 33)	1 s	XN03 (n = 18)	1 s	XN04 (n = 11)	1 s	XN05 (n = 16)	1 s
Y_2O_3 (wt %)	47.21	0.91	47.53	0.61	47.96	0.43	48.83	0.18	49.16	0.36
SiO_2	0.07	0.02	0.06	0.02	0.03	0.01	0.15	0.04	0.13	0.04
P_2O_5	33.25	0.45	33.22	0.35	33.26	0.33	33.97	0.15	33.94	0.26
CaO	0.02	0.02	0.02	0.01	0.02	0.00	0.02	0.01	0.02	0.00
ThO_2	0.14	0.03	0.11	0.04	0.10	0.03	0.05	0.02	0.09	0.04
PbO	0.36	0.01	0.36	0.01	0.36	0.02	0.39	0.01	0.40	0.01
Nd_2O_3	0.19	0.02	0.18	0.04	0.17	0.02	0.03	0.01	0.05	0.01
Sm_2O_3	0.52	0.03	0.53	0.08	0.47	0.04	0.15	0.02	0.20	0.03
Gd_2O_3	2.85	0.12	3.05	0.28	2.48	0.11	1.24	0.14	1.56	0.12
Dy_2O_3	6.43	0.21	6.68	0.21	6.28	0.18	5.07	0.23	5.01	0.25
Ho_2O_3	2.28	0.08	2.39	0.14	2.12	0.08	1.61	0.07	1.74	0.07
Er_2O_3	3.01	0.12	2.97	0.16	3.05	0.10	3.35	0.10	3.28	0.08
Tm_2O_3	0.39	0.03	0.39	0.03	0.41	0.02	0.37	0.02	0.34	0.03
Yb_2O_3	2.56	0.24	2.51	0.21	2.95	0.17	2.83	0.14	2.54	0.13
Lu_2O_3	0.37	0.06	0.38	0.04	0.46	0.04	0.37	0.04	0.31	0.04
Total	99.65		100.37		100.12		98.42		98.76	
∑REE	18.60		19.08		18.38		15.01		15.02	
					Mole fractions					
$(Th,U,Pb)SiO_4$	0.003		0.003		0.003		0.003		0.004	
$(La\text{-}Sm)PO_4$	0.008		0.008		0.007		0.002		0.003	
$Ca\ (Th,U,Pb)[PO_4]_2$	0.002		0.002		0.002		0.001		0.001	
$Y,(Gd\text{-}Lu)PO_4$	0.987		0.988		0.988		0.994		0.993	
Sum	1.000		1.000		1.000		1.000		1.000	

Note. The structural formula is based on four oxygen, and the mole fractions are calculated following Pyle et al. (2001). The complete data set can be found in the supporting information. REE = rare earth element.

subhedral in shape, and vary in length from 1 to 2 cm, with typical basal sections that are 3 to 5 mm wide on each side (Figure 2). The crystals have large homogeneous domains separated by fracture planes. Some grains may show densely fractured domains, also marked by a number of pits and minor mineral inclusions. The homogeneous domains are invariably translucent under the optical microscope and free of inclusions. BSE images of a whole crystal (Figure 3) show oscillatory zoning (due to crystal growth) and some fractured domains. On the other hand, small shards (100–200 μm) from the megacrysts are homogeneous in BSE images, which suggests that they are likely to be homogeneous in major/minor element concentrations (discussed later) at a smaller scale. Some domains with alteration, mainly along cleavage planes, can be seen with BSE but they are easily avoided under transmitted light during LA-ICP-MS analysis.

The composition corresponds to xenotime-(Y), with Y_2O_3 and P_2O_5 contents that vary from 45.7 to 50.2 wt % and 32.66 to 34.35 wt %, respectively (EPMA results—supporting information). All samples have relatively high amounts of Dy_2O_3 (5.01 to 6.68 wt %) and Er_2O_3 (2.97 to 3.35 wt %) and low Lu_2O_3 (0.31 to 0.46 g/wt %) contents. Among the non-REE elements, PbO, CaO, and ThO_2 occur in low concentrations, with PbO showing the highest values, from 0.36 to 0.40 wt % (Table 2). This is consistent with the calculated mole fractions, where the huttonite, brabantite, and monazite end-members are negligible (Table 2).

Tests for chemical homogeneity via electron microprobe were done through profiles across three different crystal fragments from each of the five samples selected for this study. The results show that each fragment is internally homogeneous and does not show any zoning pattern. Different crystals generally have comparable chemical compositions. Small variations were observed between crystals for Y_2O_3 (47.21 to 49.16 wt %) and ThO_2 (0.05 to 0.14 wt %). Light rare earth element (LREE) concentrations were below detection limit for this technique.

The internal compositional variation of the individual fragments was also assessed by LA-SF-ICP-MS. The average values obtained for each crystal are presented in Table 3.

Table 3
Average Trace Element Concentrations (μg/g) of the Studied Xenotimes Determined by LA-SF-ICP-MS on Mount M1

Sample	^{44}Ca	^{85}Rb	^{88}Sr	^{90}Zr	^{93}Nb	^{137}Ba	^{139}La	^{140}Ce	^{141}Pr	^{146}Nd	^{147}Sm	^{151}Eu	^{157}Gd	^{159}Tb
XN01 (*n* = 10)	341	57	48	119	0.98	1.3	9.1	109	102	2,256	7,281	3,275	32,106	10,402
SD	104	3.3	4.7	16	0.08	0.24	1.2	17	11	176	331	238	1,873	510
RSD%	30.4	5.8	9.7	13.3	8.0	19.1	13.6	16.1	11.3	7.8	4.5	7.3	5.8	4.9
XN02 (*n* = 10)	293	54	43	80	0.95	1.0	7.7	91	91	2,008	6,303	3,207	26,904	8,781
SD	47	2.5	2.1	49	0.09	0.28	0.95	3.9	4.4	102	349	241	1,829	544
RSD%	16.1	5	5.0	61.4	9.1	27.0	12.4	4.3	4.9	5.1	5.5	7.5	6.8	6.2
XN03 (*n* = 10)	269	50	35	30	0.9	1.1	6.1	73	81	1,801	5,619	2,850	25,158	8,213
SD	78	1.8	1.8	4.97	0.08	0.45	1.0	6.9	5.1	102	268	168	1,343	351
RSD%	28.9	3.6	5.0	16.4	8.4	39.7	16.5	9.5	6.3	5.7	4.8	5.9	5.3	4.3
XN04 (*n* = 10)	242	52	38	29	1.0	1.2	7.8	94	96	2,261	6,576	3,517	31,622	9,985
SD	52	3.0	2.6	3.8	0.06	0.34	1.1	13	18	410	376	266	3,759	909
RSD%	21.4	5.8	7.0	13.0	6.4	28.5	13.4	14.3	19.0	18.2	5.7	7.6	11.9	9.1
XN05 (*n* = 10)	311	51	39	90	1.0	1.0	8.8	103	94	2,222	6,910	3,024	30,911	9,628
SD	85	3.4	6.1	28	0.07	0.32	1.3	16	14	261	483	170	2,240	625
RSD%	27.4	6.7	15.6	31.3	7.4	30.8	14.8	15.4	15.2	11.8	7.0	5.6	7.2	6.5
NIST610 (*n* = 21)	87,308	383	507	513	456	439	463	437	454	443	472	447	466	453
SD	4,830	24	32	122	27	27	33	31	29	35	43	31	34	30
RSD%	5.5	6.1	6.3	23.8	5.9	6.1	7.0	7.0	6.5	7.9	9.2	7.0	7.4	6.6
Reference values[a]	81,476	425.7	515.5	448	465	452	440	453	448	430	453	447	449	437
BCR (*n* = 12)	50,538	46	337	180	12	685	25	53	6.9	28	6.5	2.0	6.7	1.1
SD	1,240	1.8	12	34	0.71	33	1.2	2.8	0.27	1.3	0.62	0.13	0.85	0.12
RSD%	2.5	3.9	3.5	18.8	5.7	4.8	4.7	5.2	3.9	4.6	9.4	6.5	12.6	11.6
Reference values[a]	50,844	46	337.4	186.5	12.44	683.9	25.08	53.12	6.827	28.26	6.547	1.989	6.811	1.077
BHVO (*n* = 12)	75,041	8.93	407	166	18	137	16	39	5.4	24	6.2	1.9	6.6	0.87
SD	4,350	0.56	18	33	1.8	13	1.2	4.6	0.75	2.1	1.2	0.21	0.93	0.14
RSD%	5.8	6.3	4.5	19.9	9.8	9.6	7.5	11.6	13.9	8.7	18.8	10.8	14.1	16.5
Reference values[a]	81,690	9.52	399.2	174.6	18.53	134.4	15.44	38.08	5.419	24.78	6.165	2.053	6.285	0.9455

Note. Eu/Eu[a], $(La/Gd)_N$, and $(Gd/Lu)_N$ were calculated using normalized values by the chondritic concentrations of McDonough and Sun (1995). Li, Be, B, Sc, Ti, Zn, and As were all below 10 μg/g. The complete data set can be found in the supporting information. LA-SF-ICP-MS = Laser Ablation-Sector Field-Inductively Coupled Plasma-Mass Spectrometry.
[a]Reference values are by Jochum et al. (2016).

For the analysis of mineral compositions by LA-SF-ICP-MS, 5 analyses were obtained from each fragment, for a total of 10 laser spots per crystal (Table 3). The REE patterns from the different crystals are characterized by low chondrite-normalized LREE abundances, with relative concentrations increasing with increasing atomic number to the MREE, followed by a subhorizontal pattern from the MREE to the HREE ($(Gd/Lu)_N$ = 0.94 to 1.4; Figure 4). The chondrite-normalized REE patterns show small to moderate negative Eu anomalies (*Eu/Eu** = 0.53–0.64).

Compositions of the REE are relatively uniform within each fragment for most elements, but there are variations within and between the crystals for some LREE (La-Ce-Pr; Table 3). Larger variations can also be observed for the concentrations of U and Th, with the lowest values of U found in crystal XN04 (357 μg/g) and Th in the XN01 crystal (441 μg/g). The highest contents of U and Th are found in crystals XN01 (878 μg/g of U) and XN04 (1991 μg/g of Th). The average Th/U ratios range from 1.3 to 2.7.

4.2. Isotopic Characterization

4.2.1. U-Pb Geochronology by LA-ICP-MS

Due to the oscillatory zoning observed on BSE images, we have conducted five different laser ablation profiles by LA-MC-ICP-MS on the XN03 crystal (mount M2). The profiles consisted of horizontal and vertical transverses of 10 to 15 laser spots, across and within different domains (lighter and darker ones on the BSE image), in order to assess U-Pb isotopic heterogeneity (Figure 3b). The results produced individual spot dates of 507 and 516 Ma (*n* = 54), within uncertainty of the 1% precision (at 2 s) of the technique (Figure 3b and Table 4).

Table 3 *(continued)*

^{163}Dy	^{165}Ho	^{166}Er	^{169}Tm	^{172}Yb	^{175}Lu	^{178}Hf	^{181}Ta	^{182}W	^{206}Pb	^{232}Th	^{238}U	Th/U	Eu/Eu^{a}	$(La/Gd)_N$	$(Gd/Lu)_N$
79,605	19,029	37,243	7,155	46,734	4,240	14	2.3	3.2	218	891	714	1.26	0.55	4,200	0.94
3,649	850	2,244	575	6,212	528	1.1	0.27	0.50	42	226	117	0.32	0.05	781	0.14
4.6	4.5	6.0	8.0	13.3	12.5	8.4	11.6	15.6	19.3	25.4	16.4	25.1	8.6	18.6	14.9
70,681	16,861	41,145	5,721	41,121	3,393	9.6	2.3	2.6	233	1,040	644	1.64	0.64	4,184	0.98
3,581	1,273	1,688	591	2,131	327	0.88	0.23	0.18	14	187	72	0.38	0.02	518	0.10
5.1	7.6	4.1	10.3	5.2	9.6	9.2	10.2	6.8	6.2	18.0	11.2	23.0	3.2	12.4	10.4
64,465	17,311	38,558	4,898	35,548	2,871	8.6	2.0	2.6	206	1,163	664	1.76	0.62	4,911	1.08
3,788	936	2,405	320	2,414	210	0.55	0.24	0.13	26	133	102	0.11	0.02	817	0.06
5.9	5.4	6.2	6.5	6.8	7.3	6.4	11.7	4.9	12.5	11.4	15.4	6.3	3.3	16.6	5.2
74,045	17,460	35,715	5,357	35,468	2,865	10	2.0	2.3	144	1,283	474	2.70	0.61	4,815	1.36
6,531	1,301	3,854	519	2,461	225	1.3	0.27	0.36	19	385	49	0.68	0.06	825	0.12
8.8	7.5	10.8	9.7	6.9	7.8	12.4	13.7	16.0	13.2	30.0	10.3	25.2	9.4	17.1	9.1
74,470	16,971	33,898	6,281	38,302	3,423	11	2.0	2.4	212	1,170	682	1.72	0.53	4,192	1.12
3,930	859	2,218	663	6,373	651	0.90	0.17	0.37	33	358	95	0.43	0.02	709	0.20
5.3	5.1	6.5	10.6	16.6	19.0	8.4	8.5	15.3	15.7	30.6	13.9	25.1	4.3	16.9	17.9
496	482	481	472	509	480	416	486	424	373	476	452	1.06	2.88	0.84	0.12
35	34	33	29	38	38	38	35	43	37	48	59	0.07	0.16	0.05	0.01
7.0	7.1	6.9	6.1	7.4	7.9	9.1	7.3	10.2	9.8	10.2	13.0	6.4	5.4	5.7	5.7
437	449	455	435	450	439	435	446	444	426	457.2	461.5	1.0	3.0	0.82	0.13
6.5	1.3	3.7	0.54	3.4	0.52	5.0	0.80	0.47	11	5.8	1.7	3.5	0.91	3.16	1.82
0.41	0.21	0.27	0.08	0.34	0.14	0.60	0.17	0.06	0.60	0.22	0.09	0.18	0.08	0.36	0.84
6.3	16.1	7.4	14.4	10.2	26.6	11.9	20.8	12.1	5.7	3.7	5.4	5.1	8.8	11.4	46.1
6.424	1.313	3.67	0.5341	3.392	0.5049	4.972	0.785	0.465	10.59	5.828	1.683	3.5	0.90	3.1	1.7
5.1	1.0	2.4	0.31	1.9	0.25	4.1	1.1	0.36	1.9	1.2	0.45	2.7	0.93	2.0	3.74
0.85	0.14	0.40	0.07	0.49	0.10	0.66	0.14	0.18	0.22	0.08	0.04	0.28	0.1	0.22	1.81
16.6	13.7	16.6	21.5	26.1	37.8	16.3	12.3	51.5	11.3	6.5	9.8	10.6	10.9	10.8	48.6
5.272	0.9839	2.501	0.3289	1.987	0.2775	4.44	1.174	0.212	2.037	1.225	0.4182	2.9	1.00	2.1	2.8

Following confirmation of internal homogeneity using XN03 as a proxy, random fragments of the Datas xenotime (XN01 to XN05; mount M1) were analyzed in three different analytical sessions using LA-Q-ICP-MS, LA-SF-ICP-MS, and LA-MC-ICP-MS instruments at UFOP to check the session repeatability and overall reproducibility of the dates. All the data were acquired on the same epoxy mount (M1). Uncertainties are here reported at 95% confidence level and presented as α/β, where α is the within session sample weighted mean uncertainty and β is the weighted mean uncertainty (α) plus systematic uncertainties (Horstwood et al., 2016). A summary of the U-Pb dates is shown in Figures 5–7 both as concordia diagrams and weighted average ^{206}Pb/^{238}U plots. An unweighted average summary for the five crystals on each equipment is shown in Table 4, while the complete data set is available in the supporting information.

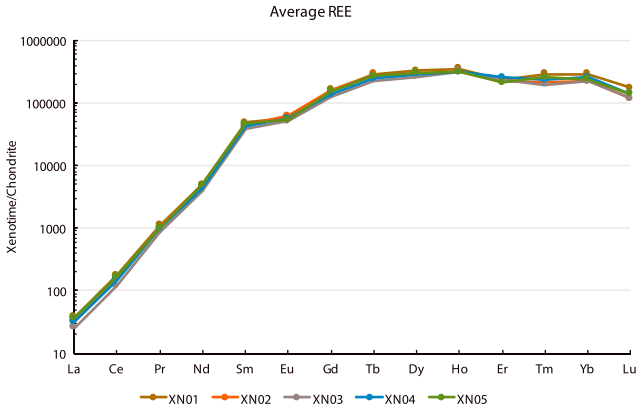

Figure 4. Chondrite-normalized average REE patterns for each crystal. The complete data are presented in the supporting information. Concentrations were normalized by the chondrite values from McDonough and Sun (1995). REE = rare earth element.

For the quadrupole instrument (Figure 5 and Table 4), ^{206}Pb/^{238}U weighted average dates ranged from 507 ± 5/11 Ma (XN04; mean square weighted deviation, *MSWD* = 0.35; *n* = 9) to 513 ± 4/11 Ma (XN05; *MSWD* = 0.23; *n* = 13). Repeatability of the ^{206}Pb/^{238}U dates was better than 0.8%, especially for the XN01 (0.6%), XN02 (0.5%), and XN03 (0.5%) crystals. For the sector field single collector (Figure 6 and Table 4), weighted average ^{206}Pb/^{238}U dates ranged from 508 ± 2/8 Ma (XN03; *MSWD* = 0.89; *n* = 31) to 521 ± 2/8 Ma (XN05; *MSWD* = 0.33; *n* = 25). Similarly, the repeatability was better than 1.0% and as low as 0.5% for the XN01 crystal. For the multicollector (Figure 7 and Table 4), weighted average dates are also within the same range of the previous data, between 513 ± 2/6 Ma (XN03; *MSWD* = 1.4; *n* = 6) and 517 ± 1/5 Ma (XN04; *MSWD* = 0.08; *n* = 6). The higher precision of this technique (Lana et al., 2017) allowed a repeatability better than 0.5%.

Geochemistry, Geophysics, Geosystems

10.1029/2017GC007412

Table 4
U-Pb Results for Each Profile Performed on XN03 in Mount M2

Departamento de Geologia, Universidade Federal de Ouro Preto					Data for Wetherill plot					Apparent dates (Ma)									
Identifier	^{206}Pb (cps)	U	Th/U	^{206}PbC (%)	^{207}Pb/^{235}U	1 s%	^{206}Pb/^{238}U	1 s %	Rho	^{207}Pb/^{206}Pb	2 s abs	2 s_{sys} abs	^{206}Pb/^{238}U	2 s abs	2 s_{sys} abs	^{207}Pb/^{235}U	2 s abs	2 s_{sys} abs	% conc
LA-MC-ICP-MS		(μg/g)																	
XN03																			
Profile 1 (n = 13)	13,573	1,297	0.84	0.02	0.6571	0.51	0.0829	0.37	0.74	512	15	19	513	4	6	513	4	6	100.2
Profile 2 (n = 12)	14,057	2,137	0.70	0.01	0.6619	0.52	0.0833	0.38	0.75	516	15	19	516	4	6	516	4	6	100.0
Profile 3 (n = 8)	10,107	2,652	0.59	0.04	0.6598	0.59	0.0831	0.38	0.59	514	20	23	515	4	6	514	5	6	100.0
Profile 4 (n = 8)	12,997	3,372	0.72	0.06	0.6571	0.61	0.0828	0.38	0.57	513	21	24	513	4	6	513	5	6	100.0
Profile 5 (n = 6)	12,991	3,362	0.74	0.09	0.6593	0.67	0.0831	0.47	0.64	514	21	24	514	5	7	514	5	7	100.1
Profile 6 (n = 7)	12,608	2,053	0.78	0.02	0.6524	0.53	0.0823	0.37	0.67	510	17	20	510	4	6	510	4	6	100.0
Average (n = 54)	12,892	2,319	0.74	0.04	0.6582	0.56	0.0830	0.39	0.67	513	18	21	514	4	6	514	5	6	100.0
LA-Q-ICP-MS		(cps)																	
XN01 (n = 15)	4,837	55,923	1.2	#N/A	0.6564	2.7	0.0825	1.3	0.49	518	105	111	511	13	16	512	22	24	100.2
XN02 (n = 15)	3,162	36,444	1.3	#N/A	0.6558	2.8	0.0821	1.3	0.47	528	109	115	509	13	16	512	23	25	100.7
XN03 (n = 13)	7,146	41,736	2.4	#N/A	0.6538	2.6	0.0822	0.95	0.37	518	106	112	509	9	14	511	21	23	100.3
XN04 (n = 9)	2,014	23,354	2.1	#N/A	0.6609	3.7	0.0818	1.4	0.39	553	148	155	507	14	17	515	31	32	101.7
XN05 (n = 13)	1,527	17,530	1.7	#N/A	0.6594	3.3	0.0829	1.4	0.44	520	127	133	513	14	17	514	27	28	100.2
LA-SF-ICP-MS		(μg/g)																	
XN01 (n = 25)	92,121	1,505	1.9	#N/A	0.6598	1.9	0.0836	1.1	0.57	509	66	73	518	11	13	514	16	17	99.4
XN02 (n = 18)	69,374	978	1.7	#N/A	0.6551	1.9	0.0831	1.1	0.58	510	62	71	515	11	13	512	15	16	99.4
XN03 (n = 31)	79,196	970	0.89	#N/A	0.6473	1.9	0.0821	1.1	0.57	511	63	73	509	10	13	507	15	17	99.6
XN04 (n = 26)	33,477	388	1.7	#N/A	0.6615	3.6	0.0839	1.1	0.31	512	75	154	519	11	13	516	30	30	99.3
XN05 (n = 25)	45,375	565	2.0	#N/A	0.6679	1.8	0.0842	1.1	0.59	525	62	67	521	11	13	519	15	16	99.7
LA-MC-ICP-MS		(μg/g)																	
XN01 (n = 16)	14,750	1140	1.8	0.04	0.6584	0.47	0.0830	0.31	0.60	513	11	19	514	3	6	514	4	6	100.2
XN02 (n = 16)	11,682	904	1.6	0.08	0.6619	0.52	0.0834	0.36	0.64	515	12	20	516	4	6	516	4	6	100.3
XN03 (n = 6)	18,848	1,484	1.0	0.00	0.6574	0.55	0.0829	0.34	0.50	512	16	22	513	3	6	513	4	6	100.3
XN04 (n = 6)	6,404	492	2.2	0.08	0.6641	0.71	0.0836	0.40	0.50	517	23	28	517	4	6	517	6	7	100.2
XN05 (n = 8)	7,139	549	1.9	0.03	0.6613	0.53	0.0833	0.37	0.66	515	12	20	516	4	6	515	4	6	100.0

Note. Compilation of the U-Pb results on Datas xenotime (mount M1) by LA-(Q, SF, MC)-ICP-MS. The results are presented on this table as simple averages, while weighted averages are presented on the text. The complete data set can be found in supporting information. The 2 s is the within session uncertainty (at 95% confidence level). The 2 sys is the within session uncertainty plus systematic uncertainties (primary reference material uncertainty and long-term variance of validation materials).

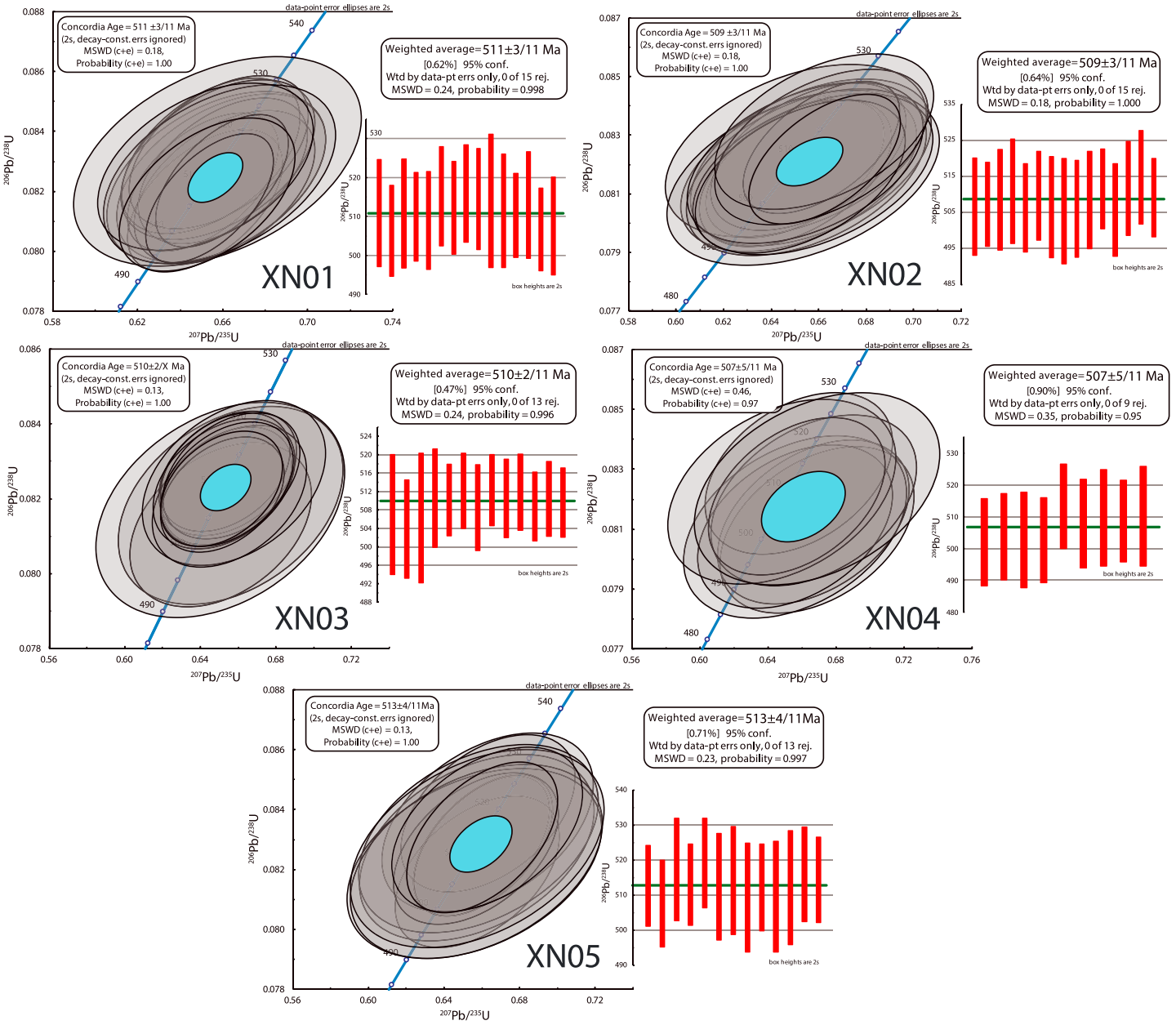

Figure 5. U-Pb isotopic data for different Datas xenotime crystals obtained by Laser Ablation-Quadrupole-Inductively Coupled Plasma-Mass Spectrometry on mount M1 and presented as both concordia and weighted averages $^{206}Pb/^{238}U$ ages. MSWD and probability of the concordia plots are of data concordance plus equivalence (c + e). Results are reported at 2 s with respective measurement and systematic uncertainties. MSWD = mean square weighted deviation.

The resulting dates from each session are concordant to subconcordant and, although they are not identical, they agree within the precision of the LA-ICP-MS instruments (>1% 2 s). Overall reproducibility was better than 0.63% for all the samples. Thus, we have selected two of the five crystals (XN01 and XN02) with the best overall reproducibility (0.47% for both) to be tested by high-precision Isotope Dilution-Thermal Ionization Mass Spectrometry (ID-TIMS).

4.2.2. U-Pb Geochronology by ID-TIMS

ID-TIMS U-Pb isotope analysis of crystals XN01 and XN02 were carried out at the University of Toronto (Jack Satterly Geochronology Laboratory) and the University of Oslo. Both laboratories received two small fragments of each of the XN01 and XN02 crystals. The analyses show variable U concentrations, from 433 to 643 μg/g for XN01 and 707 to 1,240 μg/g for XN02. The average Th/U ratios are 1.0 and 1.3, respectively.

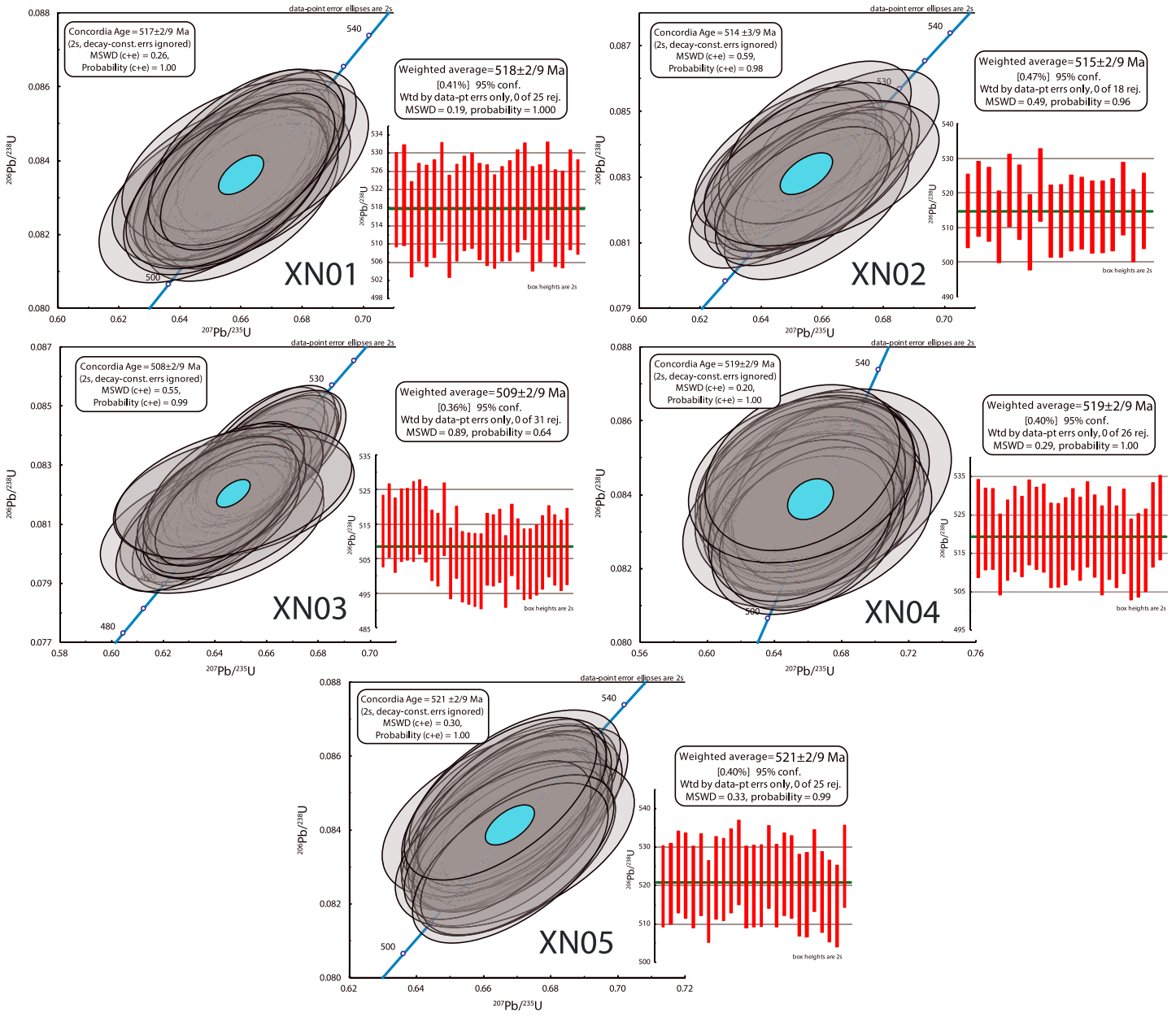

Figure 6. U-Pb isotopic data for different Datas xenotime crystals obtained by Laser Ablation-Sector Field Inductively Coupled Plasma-Mass Spectrometry and plotted as both concordia and weighted average $^{206}Pb/^{238}U$ ages. MSWD and probability of the concordia plots are of data concordance plus equivalence (c + e). Results are reported at 2 s with respective measurement and systematic uncertainties. MSWD = mean square weighted deviation.

The samples are also characterized by low common Pb contents, as reflected by high $^{206}Pb/^{204}Pb$ between 19667 and 50843, for XN01, and 14252 to 53712, for XN02 (Table 5), and total common Pb levels (blank + initial) of 1.2–2.7 pg.

U-Pb date uncertainties (at 95% confidence level) are reported as ±*x*/*y*/*z*, where *x* is the random uncertainty, *y* includes the systematic tracer uncertainty, and *z* is both tracer and decay constant uncertainties (Schoene et al., 2006). The three aliquots (obtained from the two fragments) analyzed in the JSGL (Toronto) are concordant and produced a weighted average $^{206}Pb/^{238}U$ date of 513.3 ± 1.0/1.1/1.2 Ma (*MSWD* = 7.4; *n* = 3) for XN01, and 515.4 ± 0.3/0.6/0.8 Ma (*MSWD* = 0.9; *n* = 3) for XN02. The data from Oslo also produced concordant U-Pb ages and yielded weighted average $^{206}Pb/^{238}U$ dates of 513.7 ± 5.1/5.1/5.1 Ma (*MSWD* = 1.3; *n* = 2) and 515.1 ± 5.9/5.9/5.9 Ma (*MSWD* = 1.6; *n* = 2) for XN01 and XN02, respectively (Figure 8). The relatively high

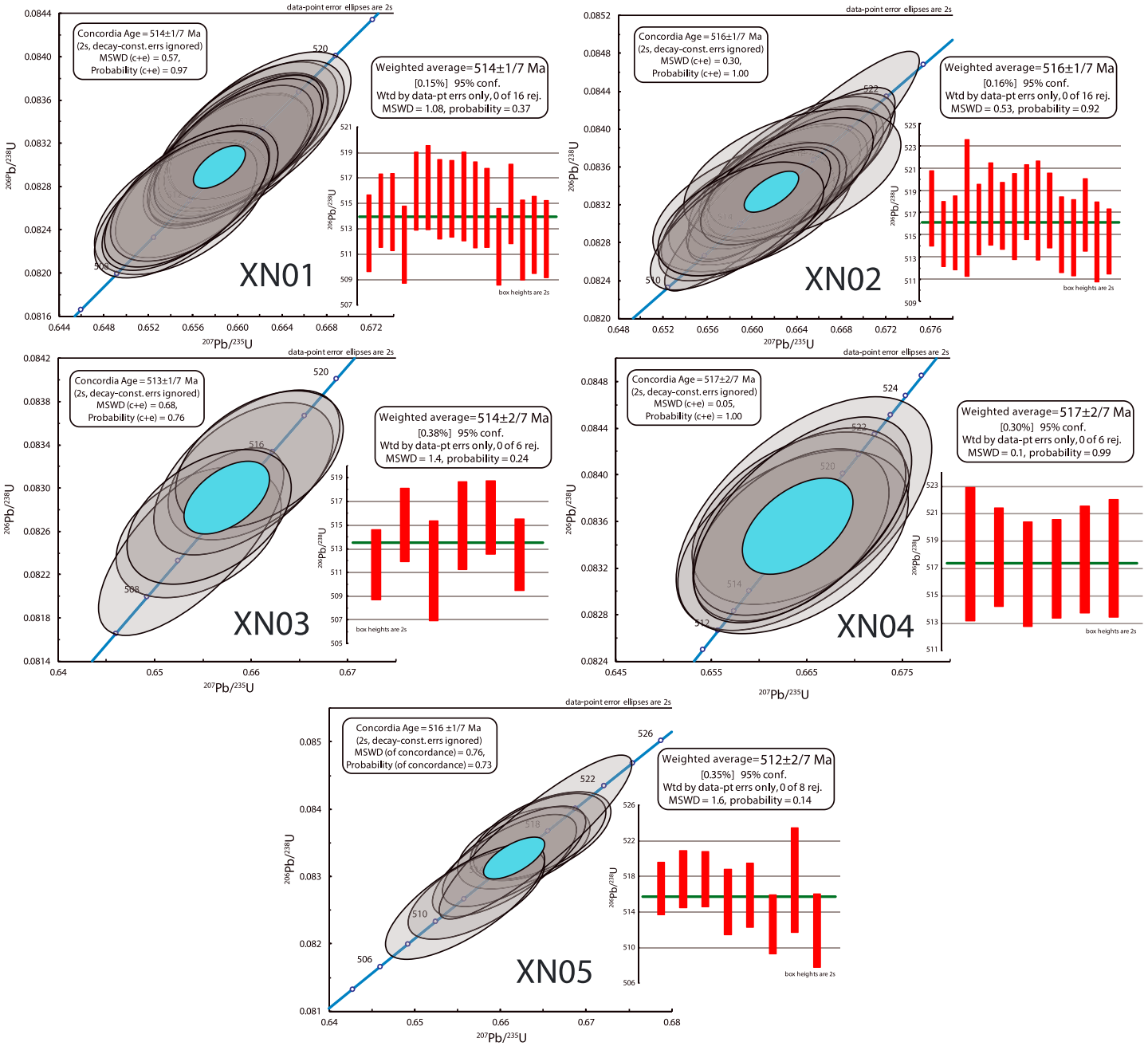

Figure 7. U-Pb isotopic data for different Datas xenotime crystals obtained by Laser Ablation-Multicollector-Inductively Coupled Plasma-Mass Spectrometry and plotted as both concordia and weighted averages $^{206}Pb/^{238}U$ ages. MSWD and probability of the concordia plots are of data concordance plus equivalence (c + e). Results are reported at 2 s with respective measurement and systematic uncertainties. MSWD = mean square weighted deviation.

MSWD for the XN01 data from Toronto suggests U-Pb isotope heterogeneity not observed in the data from Oslo, although they overlap within uncertainty from each other (see section 5).

For the XN01 xenotime, the combined results of both laboratories (n = 5) produced weighted average $^{206}Pb/^{238}U$, $^{207}Pb/^{235}U$ and $^{207}Pb/^{206}Pb$ dates of 513.4 ± 0.5/0.7/0.9 Ma (*MSWD* = 4.3), 513.7 ± 0.5/0.7/1.0 Ma (*MSWD* = 9.7), and 514.8 ± 1.3/1.4/1.6 Ma (*MSWD* = 5.7). For the XN02, combined $^{206}Pb/^{238}U$, $^{207}Pb/^{235}U$, and $^{207}Pb/^{206}Pb$ weighted average dates (n = 5) are 515.4 ± 0.2/0.6/0.8 Ma (*MSWD* = 0.97), 515.7 ± 0.5/0.7/1.0 Ma (*MSWD* = 3.4), and 517.0 ± 2.0/2.5/2.6 Ma (*MSWD* = 13). The recommended values proposed for both samples (ratios and dates) are summarized in Table 5.

Geochemistry, Geophysics, Geosystems

10.1029/2017GC007412

Table 5
ID-TIMS U-Pb Results for the Datas Xenotime Crystals (XN-01 and XN-02)

5 August 2016, JSGL, University of Toronto/17 July 2016, University of Oslo				Atomic ratios								Apparent dates (Ma)						
Identifier	Pbc (pg)[a]	U (μg/g)	Th/U[b]	$^{206}Pb/^{204}Pb$[c]	$^{207}Pb/^{235}U$[d]	±2 s abs	$^{206}Pb/^{238}U$[d]	±2 s abs	Error Corr[e]	$^{207}Pb/^{206}Pb$[d]	±2 s abs	$^{206}Pb/^{238}U$[d]	±2 s abs	$^{207}Pb/^{235}U$[d]	±2 s abs	$^{207}Pb/^{206}Pb$[d]	±2 s abs	% Disc[f]
XN01-1 JSLG	1.2	528	0.97	34,422	0.65925	0.00037	0.08297	0.00005	0.85	0.05763	0.00002	513.8	0.3	514.2	0.2	515.6	0.8	0.4
XN01-2 JSLG	1.2	643	0.98	29,686	0.65833	0.00026	0.08287	0.00004	0.83	0.05761	0.00001	513.2	0.2	513.6	0.2	515.1	0.6	0.4
XN01-3 JSLG	1.3	433	1.05	27,416	0.65733	0.00052	0.08280	0.00007	0.85	0.05757	0.00003	512.8	0.4	513.0	0.3	513.6	1.0	0.2
XN01-1 Oslo	1.8	598	1.05	19,667	0.65799	0.00156	0.08288	0.00017	0.95	0.05758	0.00005	513.3	1.0	513.4	1.0	513.8	1.7	0.1
XN01-2 Oslo	2.7	604	1.00	50,843	0.65868	0.00151	0.08302	0.00017	0.96	0.05755	0.00004	514.1	1.0	513.8	0.9	512.5	1.4	−0.3
Average					0.65832		0.08291			0.05759		513.5		513.6		514.1		
2SD					0.00145		0.00017			0.00007		1.0		0.9		2.5		
	Recommended values				0.65840	0.00084	0.08289	0.00008		0.05760	0.00003	513.4	0.5	513.7	0.5	514.8	1.4	
XN02-1 JSLG	1.2	944	1.30	53712	0.66216	0.00047	0.08326	0.00007	0.90	0.05768	0.00002	515.6	0.4	515.9	0.3	517.5	0.8	0.4
XN02-2 JSLG	1.3	707	1.29	33043	0.66198	0.00057	0.08321	0.00008	0.90	0.05770	0.00002	515.3	0.5	515.8	0.3	518.4	0.9	0.6
XN02-3 JSLG	1.3	720	1.31	29,785	0.66100	0.00065	0.08320	0.00009	0.88	0.05762	0.00003	515.2	0.5	515.2	0.4	515.3	1.1	0.0
XN02-1 Oslo	1.9	890	1.30	24,325	0.66092	0.00169	0.08311	0.00017	0.90	0.05768	0.00007	514.7	1.0	515.2	1.0	517.5	2.5	0.6
XN02-2 Oslo	1.8	1,240	1.30	14,252	0.66024	0.00161	0.08327	0.00017	0.92	0.05751	0.00006	515.6	1.0	514.8	1.0	511.1	2.1	−0.9
Average					0.66126		0.08321			0.05764		515.3		515.4		516.0		
2SD					0.00160		0.00013			0.00015		0.8		1.0		5.9		
	Recommended values				0.66174	0.00078	0.08323	0.00004		0.05766	0.00006	515.4	0.2	515.7	0.5	517.0	2.0	

Note. Recommended values are weighted averages and uncertainties are expressed at 95% confidence level. ID-TIMS = Isotope Dilution-Thermal Ionization Mass Spectrometry; JSGL = Jack Satterly Geochronology Laboratory.
[a]Pb_C is total amount of common Pb (in picograms); all common Pb assigned the isotopic composition of laboratory blank. [b]Th/U calculated from radiogenic $^{208}Pb/^{206}Pb$ ratio and $^{207}Pb/^{206}Pb$ data assuming concordance. [c]$^{206}Pb/^{204}Pb$ corrected for fractionation and common Pb in the spike. [d]Pb/Pb and Pb/U ratios corrected for fractionation, common Pb in the spike, and blank. [e]Error Corr is correlation coefficients of *X-Y* errors on the concordia plot. [f]Disc is percent discordance for the given $^{207}Pb/^{206}Pb$ age.

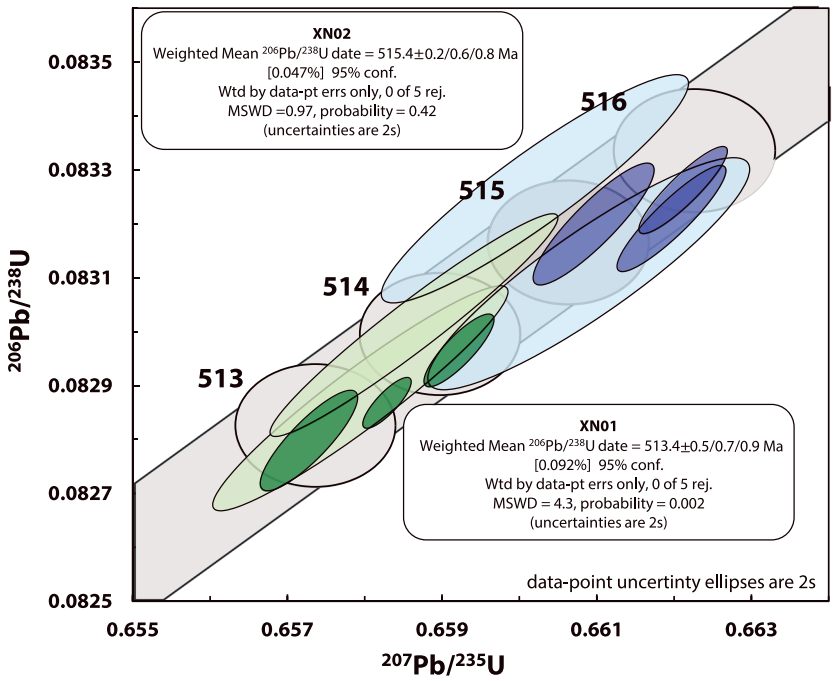

Figure 8. Isotope Dilution-Thermal Ionization Mass Spectrometry U-Pb ages of the Datas xenotime. The green ellipses are the XN01 results (light green from Oslo and dark green from JSGL) and the blue ellipses are the XN02 results (light blue from Oslo and dark blue from JSGL). The gray area is the Concordia curve including the decay constant uncertainty of Jaffey et al. (1971). JSGL = Jack Satterly Geochronology Laboratory.

5. Discussion

Xenotime crystals studied here have variable but relatively low contents of Th and U and moderate to high ∑REE (Tables 2 and 3). Even though no significant compositional zoning was detected by means of BSE imaging when looking at the small shards from the megacrysts, some alteration, mainly along cleavage planes, can be seen on BSE images. Such domains are nevertheless easily avoided under transmitted light during LA-ICP-MS analyses.

Multiple major and trace element analyses via EMPA and LA-ICP-MS show that the Datas xenotime is relatively heterogeneous but within the range of other natural xenotime RMs (e.g., Fletcher et al., 2004; Table 6). Th/U ratio determined from different aliquots of XN01 and XN02 by ID-TIMS (Table 5) have a relative variation between 3.5% (XN01) and 0.6% (XN02). In comparison, MG-1 xenotime, the main RM used globally, the relative variation in Th/U obtained by ID-TIMS is of 31% (Fletcher et al., 2004). U contents and Th/U ratios obtained by LA-SF-ICP-MS are within the range of those acquired by ID-TIMS (Tables 3 and 5). Some slightly

Table 6
Summary of Natural Xenotime Reference Materials Used/Proposed for In Situ Isotopic Analysis and Compilation of their U-Pb and Geochemical Data

Reference material	Number of ID-TIMS analyses	Number of ID-TIMS laboratories	Number of crystals analyzed by ID-TIMS	$^{206}Pb/^{238}U$ ID-TIMS age (2 s; Ma)	U (μg/g)	Th (μg/g)	∑REE (oxide wt%)	Reference
MG-1	6	1	1	490.0 ± 0.6	500–2,000	300–1,500	14.8–17.3	1, 2, and 4
BS-1	5	1	1	508.9 ± 0.6	200–1,200	2,500–6,000	19.2–21.0	1, 2, and 4
z6413 (XENO1)	5	1	5	993.8 ± 1.4	1,300–6,700	230–1,180	16.7–18.6	1, 3, 4
XN01	5	2	2	513.4 ± 0.5	433–643	1,315–5,079	18.5–20.0	5
XN02	5	2	2	515.4 ± 0.2	707–1,240	990–2,431	17.3–20.4	5

Note. References: 1, Fletcher et al., 2004; 2, Stern & Rayner, 2003; 3, Fletcher et al., 2000; 4, Cross & Williams, 2018; and 5, this study. ID-TIMS = Isotope Dilution-Thermal Ionization Mass Spectrometry; REE = rare earth element.

Geochemistry, Geophysics, Geosystems

10.1029/2017GC007412

Table 7
Round Robin Analyses Performed on Known Reference Xenotime as Unknowns Using XN01 Xenotime as Primary Reference Material by LA-MC-ICP-MS and LA-SF-ICP-MS

Round robin results for Datas xenotime at UFOP					Data for Wetherill plot					Apparent dates (Ma)								
Identifier	Comments	$\%^{206}Pb$ [a] comm	U (μg/g)	Th/U	$^{207}Pb/^{235}U$	1 *s* (%)	$^{206}Pb/^{238}U$	1 *s* (%)	Rho	$^{207}Pb/^{206}Pb$	2 *s* abs	2 s_{sys} abs	$^{206}Pb/^{238}U$	2 *s* abs	2 s_{sys} abs	$^{207}Pb/^{235}U$	2 *s* abs	2 s_{sys} abs
		LA-MC-ICP-MS																
17 July 2017																		
MG-1	*n* = 5	0.00	777	1.55	0.6255	0.51	0.0795	0.30	0.71	494	18	21	493	3	6	493	4	6
XN-02	*n* = 6	0.00	1,844	1.00	0.6607	0.46	0.0830	0.31	0.57	520	15	19	514	3	6	515	4	6
BS-1	*n* = 5	0.00	900	6.00	0.6513	0.47	0.0820	0.31	0.58	515	16	19	508	3	6	509	4	6
22 September 2017																		
MG-1	*n* = 7	0.06	854	1.00	0.6243	0.68	0.0795	0.36	0.47	491	23	27	493	3	6	493	5	7
BS-1	*n* = 5	0.01	824	6.00	0.6497	0.50	0.0822	0.31	0.54	505	13	17	509	3	6	508	4	6
XN-02	*n* = 14	0.15	1,654	1.02	0.6594	0.59	0.0830	0.31	0.45	518	18	22	514	3	6	514	5	6
8 December 2017																		
z6413	*n* = 15	0.7	316	0.11	1.5686	3.65	0.1575	3.61	0.99	993	16	19	942	63	63	956	46	46
MG-1	*n* = 6	0.01	997	0.83	0.6200	0.46	0.0790	0.30	0.54	490	11	16	490	3	5	490	4	5
LA-SF-ICP-MS																		
18 September 2017																		
XN-04	*n* = 12	0.35	730	1.00	0.66329	1.36	0.08345	1.01	0.77	516	39	46	517	10	13	517	11	14
XN-03	*n* = 13	0.04	1,700	1.65	0.64224	1.01	0.08199	0.87	0.87	484	22	31	508	9	12	504	8	11
XN-02	*n* = 12	0.04	1,453	1.93	0.65884	1.01	0.08300	0.88	0.86	513	22	32	514	9	12	514	8	11
BS-1	*n* = 14	0.21	800	6.00	0.65139	1.33	0.08200	1.01	0.78	515	37	44	508	10	13	509	11	13
MG-1	*n* = 19	0.08	900	0.80	0.61746	1.08	0.07886	0.91	0.86	483	25	37	489	9	12	488	8	12

Note. The complete data set can be found in supporting information. The 2 s is the within session uncertainty (at 95% confidence level). The 2 sys is the within session uncertainty plus systematic uncertainties (primary reference material uncertainty and long term variance of validation materials).
[a]The $\%^{206}Pb$ is the percent of common Pb of total ^{206}Pb in the analysis.

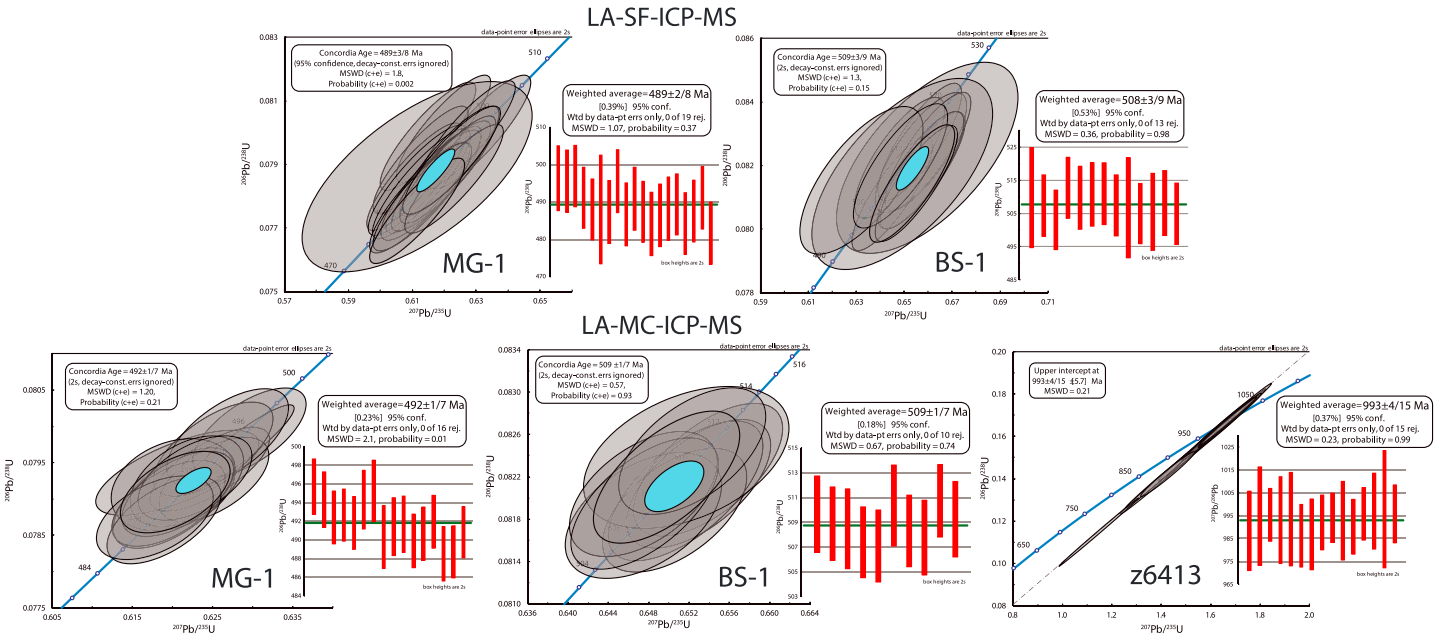

Figure 9. Results of reference xenotimes analyzed as unknowns using the XN01 xenotime as primary reference material by LA-(SF, MC)-ICP-MS at Universidade Federal de Ouro Preto plotted as both concordia and weighted averages $^{206}Pb/^{238}U$ ages ($^{207}Pb/^{206}Pb$ for the z6413 xenotime). MSWD and probability of the concordia plots are of data concordance plus equivalence (c + e). Results are reported at 2 s with respective measurement and systematic uncertainties. LA-ICP-MS = Laser Ablation-Inductively Coupled Plasma-Mass Spectrometry; MSWD = mean square weighted deviation.

higher Th/U results obtained by laser ablation are probably due to the fact that different portions of the heterogeneous megacrystal were analyzed by this method. In any case, regardless of the RM, some chemical variability is likely to be the case for all natural xenotimes (Cross & Williams, 2018; Fletcher et al., 2004, 2000; Stern & Rayner, 2003).

The ID-TIMS U-Pb isotope data of the XN01 crystal show a minor heterogeneity that was only detected by the higher-precision results from the Toronto laboratory. Despite that, the results from both Oslo and Toronto gave a weighted average $^{206}Pb/^{238}U$ date of 513.4 ± 0.5 Ma (2 s). The data for the XN02, on the other hand, mostly overlap and produced a weighted average $^{206}Pb/^{238}U$ date 515.4 ± 0.2 Ma (2 s). These dates are interpreted here as crystallization ages. Additional U-Pb data collected for these crystals by LA-(Q,SF,MC)-ICP-MS techniques show that they are sufficiently homogeneous at the precision of >1% (2 s), yielding concordant U-Pb isotope data with $^{206}Pb/^{238}U$ dates within uncertainties of those determined by ID-TIMS.

To assess the suitability of the Datas xenotime crystals as a primary RM, we have used XN01 to date other RMs (xenotime MG-1, BS-1 and z6413 from Fletcher et al., 2004; Stern & Rayner, 2003), treated as unknowns. Operating conditions were identical to the previous LA-(SF, MC)-ICP-MS sessions. For data reduction purposes, it was assumed that the XN01 had the weighted average common Pb-corrected isotopic ratios of the ID-TIMS results from both Oslo and Toronto (Table 5). Analysis of MG-1 and BS-1 xenotimes via LA-MC-ICP-MS yielded a weighted mean $^{206}Pb/^{238}U$ dates of 492 ± 1/5 Ma (95% c.l.; *MSWD* = 2.4; *n* = 18) and 509 ± 1/5 Ma (95% c.l.; *MSWD* = 0.67; *n* = 10), respectively (Table 7 and Figure 9). The z6413 data were slightly discordant; however, the upper intercept of 993 ± 4/11 Ma (95% c.l., *MSWD* = 0.21, *n* = 15) is identical to its reference age (Stern & Rayner, 2003; Table 7 and Figure 9). Ablation via LA-SF-ICP-MS on the MG-1 and BS-1 RMs yielded a weighted mean $^{206}Pb/^{238}U$ date of 489 ± 2/8 Ma (95% c.l.; *MSWD* = 1.07; *n* = 19) and 508 ± 3/8 Ma (95% c.l.; *MSWD* = 0.38; *n* = 14), respectively (Table 7 and Figure 9). The results obtained by using the XN01 Datas xenotime crystal as primary RM are in excellent agreement with the published values for MG-1, BS-1 and z6413 xenotimes (Fletcher et al., 2004; Stern & Rayner, 2003; Table 6), again demonstrating that at the precision of >1% (2 s), the Datas crystal is sufficiently homogeneous.

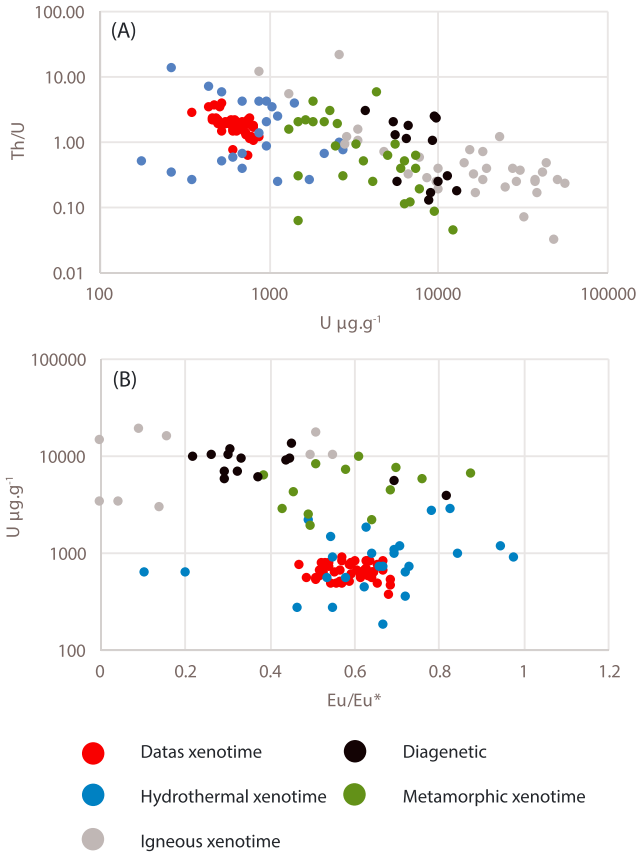

Figure 10. Plots of Th/U versus U content (a) and U content versus Eu/Eu*(b) for the Datas and other xenotime from different sources. Metamorphic—Rasmussen et al. (2011) and Franz et al. (1996); diagenetic—Rasmussen et al. (2011) and Kositcin et al. (2003); igneous—Kositcin et al. (2003) and Förster (1998); and hydrothermal—Lan et al. (2013) and Kositcin et al. (2003).

These results attest to the suitability of the Datas xenotime as a primary RM for U-Pb geochronology by LA-ICP-MS. Moreover, the reproducibility observed for the XN03, XN04, and XN05 crystals indicate that they are potential RMs for further ID-TIMS characterization. Future full characterization to develop these, and other Datas crystals, will be undertaken as the need arises, depending on the demand for aliquots of XN01 and XN02 crystal fragments.

The Datas xenotime has a higher U content than the BS-1 xenotime (Table 6), producing higher count rates and consequently better analytical precision, especially when small beam spots are required. Compared to MG-1, despite the similar U contents, the higher ∑REE concentration of the Datas xenotime (similar to BS-1) would require less matrix corrections if used on a SIMS instrument (against several percent when using MG-1; Cross & Williams, 2018; Fletcher et al., 2004; Table 6). These features make the Datas xenotime a suitable RM with similar analytical attributes as MG-1 and BS-1. Moreover, the use of the Datas xenotime as a primary U-Pb RM for in situ applications would be especially valuable for dating low-temperature hydrothermal and diagenetic events (e.g., Rasmussen, 2005; Rasmussen et al., 2010), polymetallic ore deposits (e.g., Cabral et al., 2011; Koglin et al., 2014; Zi et al., 2015), pegmatites (e.g., Thöni et al., 2008), metamorphism (e.g., Aleinikoff et al., 2015; Franz et al., 1996; Hetherington et al., 2008; Rasmussen et al., 2011), among other geological circumstances were xenotime is a petrographically characterized U-bearing mineral.

5.1. Implications on the Origin of the Datas Xenotime

Several authors have used the xenotime composition in order to distinguish its origin (e.g., Kositcin et al., 2003; Lan et al., 2013; McNaughton & Rasmussen, 2018; Rasmussen et al., 2011; Tartèse et al., 2015; Vallini et al., 2005). By comparing the composition of XN01–XN05 (Table 3) against other xenotimes, we observed a higher correlation between the Datas xenotime and hydrothermal xenotime studied by Lan et al. (2013) and Kositcin et al. (2003), even though there are some overlaps between the hydrothermal data from the literature and some metamorphic and igneous xenotime data (Figure 10). Indeed, only by means of U and Th/U contents, most xenotime formation environment overlap according to the recent diagram proposed by McNaughton and Rasmussen (2018—not shown). In a similar way to that of monazite, igneous xenotime has a pronounced negative Eu/Eu* anomaly, while diagenetic and hydrothermal xenotime usually do not (e.g., Aleinikoff et al., 2015; Kositcin et al., 2003). In a plot of Eu/Eu* anomaly against U contents, the hydrothermal origin of the xenotime becomes more evident (Figure 10), even though the Europium anomaly is variable and some of the hydrothermal data from the compilation overlap with a metamorphic origin. The chondrite-normalized REE pattern of the Datas xenotime (Figure 11) also shows some similarities between the pattern of the hydrothermal xenotime, with a relative depletion of LREE and a less pronounced Eu/Eu* anomaly, but, again, the results do not completely agree and some overlap with other formation environments occur.

As the identification of the origin of the Datas xenotime does not seem to be possible solely on a geochemical basis, a petrographic approach could also be used. Centimeter-scale xenotime crystals are usually rare, most commonly being found as ~50-µm grains or smaller (e.g., McNaughton & Rasmussen, 2018; Rasmussen, 2005). The sampling area of the alluvial Datas deposit is dominated by low-grade metasedimentary sequences (e.g., Chemale et al., 2012; Figure 1). It is highly unlike that centimeter-scale xenotime could have originated by diagenetic or metamorphic processes within these rocks. On the other hand, the area has abundant quartz veins crosscut these metasediments and bear centimeter-scale minerals, such as monazite and rutile (e.g., Gonçalves et al., 2018; Scholz et al., 2012), even if no xenotime-bearing quartz vein has yet been described. Quartz vein that bear centimeter-scale xenotimes are described in the Novo Horizonte

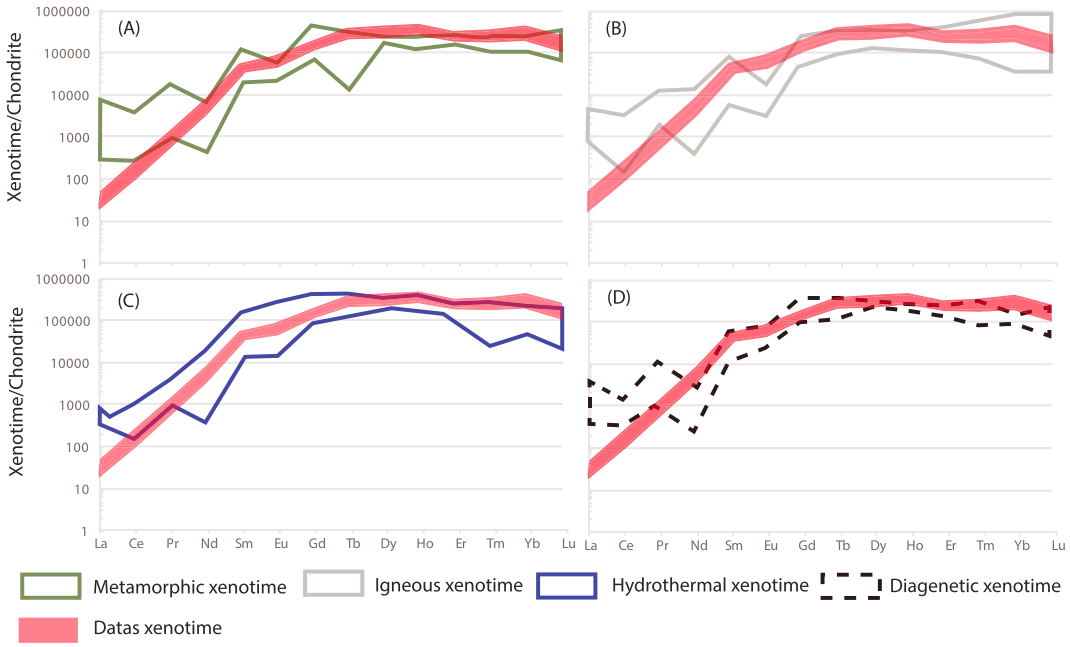

Figure 11. Rare earth element patterns for the Datas xenotime crystals and other xenotimes from different origins: (a) metamorphic (Franz et al., 1996; Rasmussen et al., 2011); (b) igneous (Förster, 1998; Kositcin et al., 2003); (c) hydrothermal (Kositcin et al., 2003; Lan et al., 2013); and (d) diagenetic (Kositcin et al., 2003; Rasmussen et al., 2011). Concentrations were normalized by the chondrite values from McDonough and Sun (1995).

area, toward north of the AO. The U-Pb ID-TIMS dates of one sample from that area ranges from 492 to 511 (Stern & Rayner, 2003).

These coupled geochemical/petrographic features suggest that the Datas xenotime was derived from the hydrothermal quartz veins that cross cut the metasediments in the Southern Espinhaço Range (Figure 1). Hydrothermal monazite from a few kilometers away from Datas (Diamantina; Figure 1) has been dated at circa 495 Ma via LA-ICP-MS and ID-TIMS (Gonçalves et al., 2018). Both the xenotime and monazite ages fall within the waning stages of AO (530–480 Ma), which also overlap with emplacement of many postcollisional granitoids and pegmatites (Pedrosa-Soares et al., 2011). We interpret the xenotime and monazite as the result of extensive fluid flow during the collapse phase of the orogen.

6. Conclusions

We propose the XN01 and XN02 xenotime crystals as primary RMs for U-Pb LA-ICP-MS analyses. The homogeneity of the crystals was demonstrated via multiple U-Pb analyses of the LA-(Q,SF,MC)-ICP-MS, which all agree within uncertainty, to the ID-TIMS results. Furthermore, it was possible to reproduce the ages of other known RMs when calibrated against the XN01 crystal. The average ID-TIMS $^{206}Pb/^{238}U$ date of 513.5 ± 0.5 Ma (2SE), for XN01, and 515.4 ± 0.2 Ma (2SE), for XN02, are interpreted as the crystallization age of these megacrysts and should be used as the accepted age of the RM. The relative homogeneity of U-Pb ages for the XN03, XN04, and XN05 megacrysts at the 1% precision of the LA-ICP-MS system makes them good candidates for further ID-TIMS characterization.

The EMPA and LA-SF-ICP-MS chemical analyses and petrographic features suggest that the alluvial Datas xenotime crystals have a hydrothermal origin, being sourced from the meter- to kilometer-scale quartz veins that crosscut the Southern Espinhaço Range. The age of the Datas crystals suggests multiple quartz vein emplacement during Cambrian times, matching the gravitational collapse of the AO.

We are willing to distribute fragments of these megacrysts upon request (please contact the corresponding author).

Acknowledgments

Supporting information can be found in the online version of this article. The authors would like to thank Janne Blichert-Toft for the editorial handling and David Chew, Christopher M. Fisher, and an anonymous reviewer for the constructive comments that greatly improved the manuscript. The authors would like to acknowledge funding from FAPEMIG (APQ-01448-15 and APQ-03793-16) and CNPq (302058/2015-0 and 305284/2015-0) and the Microanalysis Laboratory of the Universidade Federal de Ouro Preto, a member of the Microscopy and Microanalysis Network of Minas Gerais State/Brazil/FAPEMIG, for the mineral chemistry analyses and the SEM BSE imaging. Andrew Cross (Geoscience Australia) is thanked for providing aliquots of the MG-1, BS-1, and z6413 SIMS xenotime U-Pb reference materials to ISB. Guilherme Gonçalves acknowledges a PhD scholarship from CNPq (164970/2015-0). I. S. B. acknowledges funding from the National Foundation for Research (NRF, South Africa) *Incentives for Rated Researchers* and the CNPq (Brazil) *Science Without Borders* programs. R. Scholz is grateful to project PROPP/UFOP 2016.

References

Aleinikoff, J. N., Grauch, R. I., Mazdab, F. K., Kwak, L., Fanning, C. M., & Kamo, S. L. (2012). Origin of an unusual monazite-xenotime gneiss, Hudson Highlands, New York: SHRIMP U-Pb geochronology and trace element geochemistry. *American Journal of Science*, *312*(7), 723–765. https://doi.org/10.2475/07.2012.02

Aleinikoff, J. N., Lund, K., & Fanning, C. M. (2015). SHRIMP U-Pb and REE data pertaining to the origins of xenotime in Belt Supergroup rocks: Evidence for ages of deposition, hydrothermal alteration and metamorphism. *Canadian Journal of Earth Sciences*, *52*(9), 722–745. https://doi.org/10.1139/cjes-2014-0239

Alkmim, F. F., Marshak, S., Pedrosa-Soares, A. C., Peres, G. G., Cruz, S. C. P., & Whittington, A. (2006). Kinematic evolution of the Araçuaí–West Congo orogen in Brazil and Africa: Nutcracker tectonics during the Neoproterozoic assembly of Gondwana. *Precambrian Research*, *149*(1-2), 43–64. https://doi.org/10.1016/j.precamres.2006.06.007

Alkmim, F. F., & Martins-Neto, M. M. (2012). Proterozoic first-order sedimentary sequences of the São Francisco craton, eastern Brazil. *Marine and Petroleum Geology*, *33*(1), 127–139. https://doi.org/10.1016/j.marpetgeo.2011.08.011

Andrehs, G., & Heinrich, W. (1998). Experimental determination of REE distributions between monazite and xenotime: Potential for temperature-calibrated geochronology. *Chemical Geology*, *149*(1-2), 83–96. https://doi.org/10.1016/S0009-2541(98)00039-4

Bea, F., & Monteiro, P. (1999). Behavior of accessory phases and redistribution of Zr, REE, Y, Th, and U during metamorphism and partial melting of metapelites in the lower crust: An example from the Kinzigite Formation of Ivrea-Verbano, NW Italy. *Geochimica et Cosmochimica Acta*, *63*(7-8), 1133–1153. https://doi.org/10.1016/S0016-7037(98)00292-0

Buick, I. S., Hermann, J., Williams, I. S., Gibson, R. L., & Rubatto, D. (2006). A SHRIMP U-Pb and LA-ICPMS trace element study of the petrogenesis of garnet-cordierite-orthoamphibole gneisses from the Central Zone of the Limpopo Belt, South Africa. *Lithos*, *88*(1-4), 150–172. https://doi.org/10.1016/j.lithos.2005.09.001

Cabral, A. R., Lehmann, B., Tupinambá, M., Wiedenbeck, M., & Brauns, M. (2011). Geology, mineral chemistry and tourmaline B isotopes of the Córrego Bom Sucesso area, southern Serra do Espinhaço, Minas Gerais, Brazil: Implications for Au–Pd–Pt exploration in quartzitic terrain. *Journal of Geochemical Exploration*, *110*(3), 260–277. https://doi.org/10.1016/j.gexplo.2011.06.007

Chemale, F. Jr., Dussin, I. A., Alkmim, F. F., Martins, M. S., Queiroga, G., Armstrong, R., & Santos, M. N. (2012). Unravelling a Proterozoic basin history through detrital zircon geochronology: The case of the Espinhaço Supergroup, Minas Gerais, Brazil. *Gondwana Research*, *22*(1), 200–206. https://doi.org/10.1016/j.gr.2011.08.016

Cherniak, D. J. (2006). Pb and rare earth element diffusion in xenotime. *Lithos*, *88*(1-4), 1–14. https://doi.org/10.1016/j.lithos.2005.08.002

Cross, A. J., & Williams, I. S. (2018). SHRIMP U-Pb-Th xenotime (YPO_4) geochronology: A novel approach for the correction of SIMS matrix effects. *Chemical Geology*, *484*, 81–108. https://doi.org/10.1016/j.chemgeo.2017.12.017

Dahl, P. S. (1997). A crystal-chemical basis for Pb retention and fission-track annealing systematics in U-bearing minerals, with implications for geochronology. *Earth and Planetary Science Letters*, *150*(3-4), 277–290. https://doi.org/10.1016/S0012-821X(97)00108-8

Dalquist, J. A. (2001). REE fractionation by accessory minerals in epidote-bearing metaluminous granitoids from the Sierras Pampeanas, Argentina. *Mineralogical Magazine*, *65*(4), 463–475. https://doi.org/10.1180/002646101750377506

Emden, B., van Thornber, M. R., Graham, J., & Lincoln, F. J. (1997). The incorporation of actinides in monazite and xenotime from placer deposits in Western Australia. *Canadian Mineralogist*, *35*, 95–104.

Fisher, C. M., Hanchar, J. M., Miller, C. F., Vervoort, J. D., & Whitehouse, M. J. (2017). Combining Nd isotopes in monazite and Hf isotopes in zircon to understand complex open-system processes in granitic magmas. *Geology*, *45*(3), 267–270. https://doi.org/10.1130/G38458.1

Fletcher, I. R., McNaughton, N. J., Aleinikoff, J. A., Rasmussen, B., & Kamo, S. L. (2004). Improved calibration procedures and new standards for U–Pb and Th–Pb dating of Phanerozoic xenotime by ion microprobe. *Chemical Geology*, *209*(3-4), 295–314. https://doi.org/10.1016/j.chemgeo.2004.06.015

Fletcher, I. R., Rasmussen, B., & McNaughton, N. J. (2000). SHRIMP U–Pb geochronology of authigenic xenotime and its potential for dating sedimentary basins. *Australian Journal of Earth Sciences*, *46*, 845–860.

Förster, H.-J. (1998). The chemical composition of REE-Y-Th-U-rich accessory minerals in peraluminous granites of the Erzgebirge–Fichtelgebirge region, Germany, Part II: Xenotime. *American Mineralogist*, *83*(11-12 Part 1), 1302–1315. https://doi.org/10.2138/am-1998-11-1219

Franz, G., Andrehs, G., & Rhede, D. (1996). Crystal chemistry of monazite and xenotime from Saxothuringian-Moldanubian metapelites, NE Bavaria, Germany. *European Journal of Mineralogy*, *8*(5), 1097–1118. https://doi.org/10.1127/ejm/8/5/1097

Gerdes, A., & Zeh, A. (2006). Combined U-Pb and Hf isotope LA-(MC-)ICP-MS analyses of detrital zircons: Comparison with SHRIMP and new constraints for the provenance and age of an Armorican metasediment in Central Germany. *Earth and Planetary Science Letters*, *249*(1-2), 47–61. https://doi.org/10.1016/j.epsl.2006.06.039

Gerdes, A., & Zeh, A. (2009). Zircon formation versus zircon alteration–new insights from combined U-Pb and Lu-Hf in-situ LA-ICP-MS analyses, and consequences for the interpretation of Archaean zircon from the Central Zone of the Limpopo Belt. *Chemical Geology*, *261*(3-4), 230–243. https://doi.org/10.1016/j.chemgeo.2008.03.005

Gerstenberger, H., & Haase, G. (1997). A highly effective emitter substance for mass spectrometric Pb isotope ration determinations. *Chemical Geology*, *136*(3-4), 309–312. https://doi.org/10.1016/S0009-2541(96)00033-2

Gonçalves, G. O., Lana, C., Scholz, R., Buick, I., Gerdes, A., Kamo, S. L., et al. (2016). An assessment of monazite from the Itambé pegmatite district for use as a U-Pb isotope reference material for microanalysis and implications for the origin of the "Moacyr" monazite. *Chemical Geology*, *424*, 30–50. https://doi.org/10.1016/j.chemgeo.2015.12.019

Gonçalves, G. O., Lana, C., Buick, I. S., Alkmim, F .F., & Scholz, R. (2017). Post-orogenic hydrothermal fluid flow in the Eastern São Francisco Craton: Implications for ore mineralization. Goldschmidt Abstracts, 2017.

Gonçalves, G. O., Lana, C., Scholz, R., Buick, I. S., Gerdes, A., Kamo, S. L., et al. (2018). The Diamantina monazite: a new low-Th reference material for microanalysis. *Geostandards and Geoanalytical Research*, *42*(1), 25–47. https://doi.org/10.1111/ggr.12192

Gregory, C. J., McFarlane, C. R. M., Hermann, J., & Rubatto, D. (2009). Tracing the evolution of calc-alkaline magma: In-situ Sm-Nd isotope studies of accessory minerals in the Bergell Igneous Complex, Italy. *Chemical Geology*, *260*(1-2), 73–86. https://doi.org/10.1016/j.chemgeo.2008.12.003

Hazarika, P., Mishra, B., Ozha, M. K., & Pruseth, K. L. (2017). An improved EPMA analytical protocol for U-Th-Pb total dating in xenotime: Age constraints from polygenetic Mangalwar Complex, Northwestern India. *Chemie der Erde-Geochemistry*. https://doi.org/10.1016/j.chemer.2017.01.010

Heinrich, W., Andrehs, G., & Franz, G. (1997). Monazite–xenotime immiscibility gap thermometry: I. An empirical calibration. *Journal of Metamorphic Geology*, *15*(1), 3–16. https://doi.org/10.1111/j.1525-1314.1997.t01-1-00052.x

Hetherington, C. J., Jercinovic, M. J., Williams, M. L., & Mahan, K. (2008). Understanding geologic processes with xenotime: Composition, chronology, and a protocol for electron probe microanalysis. *Chemical Geology*, *254*(3-4), 133–147. https://doi.org/10.1016/j.chemgeo.2008.05.020

Hiess, J., Condon, D. J., McLean, N., & Noble, S. R. (2012). $^{238}U/^{235}U$ systematics in terrestrial uranium-bearing minerals. *Science*, *335*(6076), 1610–1614. https://doi.org/10.1126/science.1215507

Horstwood, M. S. A., Košler, J., Gehrels, G., Jackson, S. E., McLean, N. M., Paton, C., et al. (2016). Community-derived standards for LA-ICP-MS U-(Th-)Pb geochronology—Uncertainty propagation, age interpretation and data reporting. *Geostandards and Geoanalytical Research*, *40*(3), 311–332. https://doi.org/10.1111/j.1751-908X.2016.00379.x

Jaffey, A. H., Flynn, K. F., Glendenin, L. E., Bentley, W. C., & Essling, A. M. (1971). Precision measurement of half-lives and specific activities of ^{235}U and ^{238}U. *Physics Review, Section C*, *4*, 1889–1906.

Jochum, K. P., Weis, U., Schwager, B., Stoll, B., Wilson, S. A., Haug, G. H., et al. (2016). Reference values following ISO guidelines for frequently requested rock reference materials. *Geostandards and Geoanalytical Research*, *40*(3), 333–350. https://doi.org/10.1111/j.1751-908X.2015.00392.x

Koglin, N., Zeh, A., Cabral, A. R., Gomes, A. A. S. Jr., Neto, A. C., Brunetto, W. J., & Galbiatti, H. F. (2014). Depositional age and sediment source of the auriferous Moeda Formation, Quadrilátero Ferrífero of Minas Gerais, Brazil: New constraints from U-Pb_Hf isotopes in zircon and xenotime. *Precambrian Research*, *255*, 96–108. https://doi.org/10.1016/j.precamres.2014.09.010

Kositcin, N., McNaughton, N. J., Griffin, B. J., Fletcher, I. R., Groves, D. I., & Rasmussen, B. (2003). Textural and geochemical discrimination between xenotime of different origin in the Archaean Witwatersrand Basin, South Africa. *Geochimica et Cosmochimica Acta*, *67*(4), 709–731. https://doi.org/10.1016/S0016-7037(02)01169-9

Lan, Z.-W., Chen, Z.-Q., Li, X.-H., Li, B., & Adams, D. (2013). Hydrothermal origin of the Paleoproterozoic xenotime from the King Leopold Sandstone of the Kimberley Group, Kimberley, NW Australia: Implications for a ca 1.7 Ga farfield hydrothermal event. *Australian Journal of Earth Sciences*, *60*(4), 497–508. https://doi.org/10.1080/08120099.2013.806360

Lana, C., Farina, F., Gerdes, A., Alkmim, A., Gonçalves, G. O., & Jardim, A. C. (2017). Characterization of zircon reference materials via high precision U-Pb LA-MC-ICP-MS. *Journal of Analytical Atomic Spectrometry*, *32*(10), 2011–2023. https://doi.org/10.1039/C7JA00167C

Liu, Z. C., Wu, F. Y., Guo, C. L., Zhao, Z. F., Yang, J. H., & Sun, J. F. (2011). In situ U-Pb dating of xenotime by laser ablation (LA)-ICP-MS. *Chinese Science Bulletin*, *56*(27), 2948–2956. https://doi.org/10.1007/s11434-011-4657-y

Ludwig, K. R. (2003). User's manual for isoplot 3.00 (70 pp.). Berkeley, CA: Berkeley Geochronology Center.

McDonough, W. F., & Sun, S.-S. (1995). The composition of the Earth. *Chemical Geology*, *120*(3-4), 223–253. https://doi.org/10.1016/0009-2541(94)00140-4

McNaughton, N. J., & Rasmussen, B. (2018). Geochemical characterization of xenotime formation enviroments using U-Th. *Chemical Geology*, *484*, 109–119. https://doi.org/10.1016/j.chemgeo.2017.08.016

Miller, C. F., Hanchar, J. M., Wooden, J. L., & Bennett, V. C. (1992). Source region of a granite batholith: evidence from lower crustal xenoliths and inherited accessory minerals. . Second Hutton Symposium: The Origin of Granites and Related Rocks. *Transactions of the Royal Society of Edinburgh*, *83*, 49–62.

Pedrosa-Soares, A. C., Campos, C., Noce, C. M., Silva, L. C., Roncato, J., Novo, T., et al. (2011). Late Neoproterozoic Cambrian granitic magmatism in the Araçuaí Orogen, the Eastern Brazilian Pegmatite Province and related mineral resources (SE Brazil). *Geological Society*, *350*(1), 25–51. https://doi.org/10.1144/SP350.3

Pyle, J. M., Spear, F. S., Rudnick, R. L., & McDonough, W. F. (2001). Monazite–xenotime–garnet equilibrium in metapelites and a new monazite–garnet thermometer. *Journal of Petrology*, *42*, 2083–2107.

Pyle, J. M., & Spear, F. S. (2000). An empirical garnet (YAG)–xenotime thermometer. *Contributions to Mineralogy and Petrology*, *138*(1), 51–58. https://doi.org/10.1007/PL00007662

Rasmussen, B. (2005). Radiometric dating of sedimentary rocks: the application of diagenetic xenotime geochronology. *Earth-Science Reviews*, *68*(3-4), 197–243. https://doi.org/10.1016/j.earscirev.2004.05.004

Rasmussen, B., Fletcher, I. R., Bengtson, S., & McNaughton, N. J. (2004). SHRIMP U–Pb dating of diagenetic xenotime in the Stirling Range Formation, Western Australia: 1.8 billion years minimum age for the Stirling biota. *Precambrian Research*, *133*(3-4), 329–337. https://doi.org/10.1016/j.precamres.2004.05.008

Rasmussen, B., Fletcher, I. R., & McNaughton, N. J. (2001). Dating low-grade metamorphic events by SHRIMP U-Pb analysis of monazite in shales. *Geology*, *29*(10), 963–966. https://doi.org/10.1130/0091-7613(2001)029<0963:DLGMEB>2.0.CO;2

Rasmussen, B., Fletcher, I. R., & Muhling, J. R. (2011). The response of xenotime to prograde metamorphism. *Contributions to Mineralogy and Petrology*, *162*(6), 1259–1277. https://doi.org/10.1007/s00410-011-0650-3

Rasmussen, B., Fletcher, I. R., Muhling, J. R., Mueller, A. G., & Hall, G. C. (2007). Bushveld-aged fluid flow, peak metamorphism, and gold mobilization in the Witwatersrand basin, South Africa: constraints from in situ SHRIMP U-Pb dating of monazite and xenotime. *Geology*, *35*(10), 931–934. https://doi.org/10.1130/G23588A.1

Rasmussen, B., Fletcher, I. R., Muhling, J. R., & Wilde, S. A. (2010). In situ U–Th–Pb geochronology of monazite and xenotime from the Jack Hills belt: Implications for the age of deposition and metamorphism of Hadean zircons. *Precambrian Research*, *180*(1-2), 26–46. https://doi.org/10.1016/j.precamres.2010.03.004

Santos, M. M., Lana, C., Scholz, R., Buick, I., Schmitz, M. D., Kamo, S. L., et al. (2017). A new appraisal of Sri Lankan zircons as reference material for in situ U-Pb geochronology, REE analyses and Lu-Hf isotope tracing. *Geostandards and Geoanalytical Research*, *41*(3), 335–358. https://doi.org/10.1111/ggr.12167

Schoene, B., Crowley, J. L., Condon, D. J., Schmitz, M. D., & Bowring, S. A. (2006). Reassessing the uranium decay constants for geochronology using ID-TIMS U-Pb data. *Geochimica et Cosmochimica Acta*, *70*(2), 426–445. https://doi.org/10.1016/j.gca.2005.09.007

Scholz, R., Chaves, M. L. S. C., Krambrock, K., Pinheiro, M. V. B., Barreto, S. B., & Menezes, M. G. (2012). Brazilian quartz deposits with special emphasis on gemstone quartz and its color treatment. In: Götze, Jens; Möckel, Robert (eds). (Org.). *Quartz, deposits, mineralogy and analytics. 1ed.* Heidelberg: Springer-Verlag, (p. 139–156).

Stacey, J. S., & Kramers, J. D. (1975). Approximation of terrestrial lead isotope evolution by a two-stage model. *Earth and Planetary Science Letters*, *26*(2), 207–221. https://doi.org/10.1016/0012-821X(75)90088-6

Stern, R. A., & Rayner, R. (2003). Age of several xenotimes megacrysts by ID-TIMS: Potential reference material for ion microprobe U-Pb geochronology. Ontario, Geological Survey of Canada, Current Research (7 pp.).

Storkey, A., Hermann, J., Hand, M., & Buick, I. S. (2005). Using in-situ trace element determinations to monitor partial melting processes in metabasites. *Journal of Petrology*, *46*(6), 1283–1308. https://doi.org/10.1093/petrology/egi017

Švecová, E., Čopjaková, R., Loso, Z., Škoda, R., Nasdala, L., & Cícha, J. (2016). Multi-stage evolution of xenotime–(Y) from Písek pegmatites, Czech Republic: an electron probe micro-analysis and Raman spectroscopy study. *Mineralogy and Petrology*, *110*(6), 747–765. https://doi.org/10.1007/s00710-016-0442-6

Takenaka, L. B., Lana, C., Scholz, R., Nalini, H. A. Jr., & Abreu, A. T. (2015). Optimization of the in-situ U-Pb age dating method via LA-Quadrupole-ICP-MS with applications to the timing of U-Zr-Mo mineralization in the Poços de Caldas Alkaline Complex, SE Brazil. *Journal of South American Earth Sciences*, *62*, 70–79. https://doi.org/10.1016/j.jsames.2015.04.007

Tartèse, R., Poujol, M., Gloaguen, E., Boulvais, P., Drost, K., Košler, J., & Ntaflos, T. (2015). Hydrothermal activity during tectonic building of the Variscan orogen recorded by U-Pb systematics of xenotime in the Grès Armoricain formation, Massif Armoricain, France. *Mineralogy and Petrology*, *109*(4), 485–500. https://doi.org/10.1007/s00710-015-0373-7

Thöni, M., Miller, C., Zanetti, A., Habler, G., & Goessler, W. (2008). Sm–Nd isotope systematics of high-REE accessory minerals and major phases: ID-TIMS, LA-ICP-MS and EPMA data constrain multiple Permian–Triassic pegmatite emplacement in the Koralpe, Eastern Alps. *Chemical Geology*, *254*(3-4), 216–237. https://doi.org/10.1016/j.chemgeo.2008.03.008

Vallini, D. A., Rasmussen, B., Krapez, B., Fletcher, I. R., & McNaughton, N. J. (2005). Microtextures, geochemistry and geochronology of authigenic xenotime: constraining the cementation history of a Palaeoproterozoic metasedimentary sequence. *Sedimentology*, *52*(1), 101–122. https://doi.org/10.1111/j.1365-3091.2004.00688.x

Van Achterbergh, E., Ryan, C. G., Jackson, S. E., & Griffin, W. L. (2001). Data reduction software for LA-ICP-MS: appendix. In P. J. Sylvester (Ed.), *Laser Ablation –ICP-Mass Spectrometry in the Earth Sciences: Principles and Applications, Mineralogical Association of Canada Short Course Series, Ottawa, Ontario, Canada* (Vol. 29, pp. 239–243).

Viskupic, K., & Hodges, K. V. (2001). Monazite-xenotime thermochronometry: Methodology and an example from the Nepalese Himalaya. *Contributions to Mineralogy and Petrology*, *141*(2), 233–247. https://doi.org/10.1007/s004100100239

Wall, F., Niku-Paavola, V. N., Storey, C., Müller, A., & Jeffries, T. (2008). Xenotime-(Y) from carbonatite dykes at Lofdal, Namibia: Unusually low LREE:HREE ratio in carbonatite, and the first dating of xenotime overgrowths on zircon. *The Canadian Mineralogist*, *46*(4), 861–877. https://doi.org/10.3749/canmin.46.4.861

Zi, J. W., Rasmussen, B., Muhling, J. R., Fletcher, I. R., Thorne, A. M., Johnson, S. P., et al. (2015). In situ U–Pb geochronology of xenotime and monazite from the Abrapolymetallic deposit in the Capricorn Orogen, Australia: Dating hydrothermal mineralization and fluid flow in a long-lived crustal structure. *Precambrian Research*, *260*, 91–112. https://doi.org/10.1016/j.precamres.2015.01.010